NASA MEMO 1-2-59L

NASA

MEMORANDUM

A METHOD FOR COMPUTING TURBULENT HEAT TRANSFER IN THE PRESENCE OF A STREAMWISE PRESSURE GRADIENT FOR BODIES IN HIGH-SPEED FLOW

By Nathaniel B. Cohen

Langley Research Center
Langley Field, Va.

NATIONAL AERONAUTICS AND SPACE ADMINISTRATION

WASHINGTON
March 1959

NATIONAL AERONAUTICS AND SPACE ADMINISTRATION

MEMORANDUM 1-2-59L

A METHOD FOR COMPUTING TURBULENT HEAT TRANSFER IN THE PRESENCE OF A STREAMWISE PRESSURE GRADIENT FOR BODIES IN HIGH-SPEED FLOW

By Nathaniel B. Cohen

SUMMARY

A method for computing the turbulent heat transfer to two-dimensional and axisymmetric bodies in high-speed flow is derived from the integrated equations of the boundary layer by utilizing a Stewartson type transformation. A modified Reynolds analogy between skin friction and heat transfer which depends upon local pressure gradient results from the analysis. Exact and approximate solutions are derived from the approximate differential equations; the exact solution is applicable for arbitrary initial (transition) conditions and the approximate solution requires fully developed turbulent flow from stagnation point or leading edge.

For the exact solution, the assumption of fully developed turbulent flow from the stagnation point yields a solution representative of a variety of arbitrary transition solutions. The exact solution (restricted to stagnation initial conditions) and the approximate solution are shown to agree within 5 percent when applied to several blunt shapes. The present solutions generally predict the measured heating rates on these bodies within the accuracy of the measurements except where transition was thought to begin in the region of the peak predicted heat transfer.

The present solutions appear to be sufficiently accurate for design purposes. The exact solution alone offers the generality of arbitrary transition; the approximate solution offers accuracy and relative simplicity but requires the assumption of stagnation-point initial conditions. Because of the scarcity of knowledge of the transition phenomenon, this latter restriction does not seriously impair the usefulness of the approximation.

INTRODUCTION

Reentry conditions at high Reynolds number and the possibility of surfaces roughened by collisions with meteoric particles and dust are conducive to the existence of turbulent boundary layers on missiles, satellites, spaceships, and similar vehicles entering a planetary atmosphere. A primary concern of the ballistic missile program, for example, is the accurate prediction of turbulent heat transfer to a blunt body in high-speed flow. This problem has inspired a great deal of research in recent years; although many approximate theories have evolved, none appears to be sufficiently general for widespread application.

The problem is the computation of turbulent heat transfer from a compressible (possibly dissociated) gas to a cold wall in the presence of a pressure gradient. Except for the case with dissociation, the zero-pressure-gradient skin friction may be computed with sufficient accuracy either from mixing length theories, for example, those of Van Driest for a plate (ref. 1) and for a cone (ref. 2), or from an empirical power law such as the Blasius law. (See, for example, ref. 3.) Compressibility in the latter case may be taken into account through a reference temperature formulation of the power law. In both methods, heat transfer is computed from the skin friction through the use of Reynolds analogy between heat transfer and skin friction suitably modified for the effect of a nonunit Prandtl number.

The presence of a pressure gradient seriously modifies the flow and the subsequent friction and heat-transfer behavior. Most recent methods of predicting the turbulent heat transfer to a body in the presence of a pressure gradient center about extensions of the inverse power law friction coefficient. Some of these are described by Libby and Cresci in reference 4. The simplest uses flat-plate skin friction and heat-transfer relations evaluated for the local flow conditions on the body in question. Rose, Probstein, and Adams (ref. 5) combine a flat-plate shear law with the complete momentum equation integrated across the boundary layer and including pressure gradient. Heat transfer is computed from the resulting skin friction through the flat-plate Reynolds analogy modified to account for Prandtl number. Reference 5 reasons that the effect of the pressure gradient on the velocity and temperature profiles is small and thus the flat-plate friction law and analogy between heat transfer and skin friction are valid.

A relation between heat transfer and skin friction including the effect of pressure gradient may be derived from the integrated momentum and energy equations. (See refs. 4, 6, and 7.) Bloom and Martellucci (ref. 6) were apparently the first to use this relation, and they combined it with an inverse power friction law and a reference enthalpy correction

for compressibility effects. The results of this method and a similar method (ref. 4) indicated predicted heat transfer lower than that found experimentally, and excessive dependence of the modified Reynolds analogy upon pressure gradient. Assumption of the validity of the Crocco form of the total enthalpy-velocity relation in the boundary layer appears to have caused this trend.

Another method of accounting for compressibility and pressure gradient was developed by Reshotko and Tucker. (See ref. 8.) This method utilizes the Stewartson transformation (ref. 9) applied to the turbulent case, a friction law including the effect of pressure gradient upon shape factor, and a Reynolds analogy factor evaluated from an approximate solution for laminar flow in reference 10. This approach is restricted to isothermal walls with adverse and small favorable pressure gradients regardless of wall temperature and to flow with large favorable pressure gradients over highly cooled surfaces. M. Richard Dennison while at Missile Systems Division of Lockheed Aircraft Corporation (in a paper not generally available) extended Van Driest's analysis to include the effect of pressure gradient upon Reynolds analogy, neglecting, however, the direct effect of pressure gradient upon the momentum equation. This assumption appears to be justified only for highly cooled surfaces. The analysis is further restricted to isothermal walls.

The present analysis attempts to correct the deficiencies of the aforementioned methods and provides a comprehensive method for the computation of turbulent heat transfer in compressible flow for high subsonic and supersonic as well as hypersonic conditions. The effect of pressure gradient is retained in the integrated momentum equation and a modified Reynolds analogy is derived. The Stewartson transformation is used to reduce these equations to a form close to the incompressible relations. An incompressible friction relation which neglects the effect of pressure gradient upon the boundary-layer shape factor is assumed to be valid in the transformed coordinate system and the compressible friction coefficient is then calculated by using a form of the reference temperature method. The heat transfer is then calculated from the friction and the modified Reynolds analogy.

This treatment includes the possibility of nonisothermal heated or cooled surfaces but is limited to favorable and small adverse pressure gradients. Although dissociation is neglected, variable specific heats may be approximated through use of a linear interpolation formula.

Heat-transfer rates predicted by the present method are compared with experimental results and with other predictions.

SYMBOLS

A_m	coefficient in friction law
a,b,c	coefficients in enthalpy-velocity relation
a_o	dimensionless stagnation velocity gradient
c_f	skin-friction coefficient, $\tau_w/\frac{1}{2}\rho_e u_e^2$
c_p	specific heat at constant pressure
c_v	specific heat at constant volume
d_1,d_2	parameters given in equations (A14) and (A15)
$F(\xi)$	function defined by $\int_0^\xi \underline{r}^{\frac{m+1}{m}} \underline{U}_e^{\frac{\Gamma(m+1)-1}{m}} d\xi$
$f_1(\xi)$	function defined by equation (65a)
$f_2(\xi)$	function defined by equation (65b)
H	total enthalpy, $h + \frac{u^2}{2}$
H^*	enthalpy difference, $H - H_w$
h	static enthalpy
k	thermal conductivity
l	reference length
M	Mach number
m	reciprocal exponent in friction law
N_{Pr}	Prandtl number, $\frac{\mu c_p}{k}$

N_{Re}	local Reynolds number, $\frac{\rho_e u_e x}{\mu_e}$
N_{Ro}	reference Reynolds number, $\frac{\rho_o \sqrt{2h_o l}}{\mu_o}$
N_{St}	Stanton number, $\frac{-q_w}{\rho_e u_e H_{aw}^*}$
n	reciprocal exponent in velocity-profile power law
p	pressure
q_w	wall heat transfer
r	body radius
T	temperature
U	velocity in X-direction in transformed plane
u	velocity in x-direction in physical plane
X	transformed coordinate along surface
x	physical coordinate along surface
Y	transformed coordinate normal to surface
y	physical coordinate normal to surface
Z	Reynolds analogy factor
α	constant in density-enthalpy correlation equation
β	pressure gradient parameter
Γ	function defined by equation (37a)
$\bar{\Gamma}$	function defined by equation (62)
γ	ratio of specific heats, c_p/c_v
Δ	transformed thickness of boundary layer
Δ_H	transformed thickness of total enthalpy boundary layer

Δ_U transformed thickness of velocity boundary layer

δ physical thickness of boundary layer

δ_H physical thickness of total enthalpy boundary layer

δ_u physical thickness of velocity boundary layer

$\bar{\delta}_1$ transformed displacement thickness, $\int_0^\infty \left(1 - \frac{U}{U_e}\right) dY$

$\bar{\delta}_2$ transformed enthalpy thickness, $\int_0^\infty \left(1 - \frac{H^*}{H_e^*}\right) dY$

δ^* displacement thickness, $\int_0^\infty \left(1 - \frac{\rho u}{\rho_e u_e}\right) dy$

η_r enthalpy recovery factor

Θ reduced momentum thickness (eq. (48a))

θ momentum thickness, $\int_0^\infty \frac{u}{u_e}\left(1 - \frac{u}{u_e}\right)\frac{\rho}{\rho_e}\, dy$

$\bar{\theta}$ transformed momentum thickness, $\int_0^\infty \frac{U}{U_e}\left(1 - \frac{U}{U_e}\right) dY$

Λ function defined by equation (37b)

$\bar{\lambda}$ transformed thickness, $\int_0^\infty \left(\frac{U}{U_e}\right)^2\left(1 - \frac{U}{U_e}\right) dY$

μ absolute viscosity

ξ transformed dimensionless length, $\frac{X}{l}$

ρ density

τ_w wall shear

φ enthalpy convection thickness, $\int_0^\infty \frac{u}{u_e}\left(1 - \frac{H^*}{H_e^*}\right)\frac{\rho}{\rho_e}\,dy$

$\overline{\varphi}$ transformed enthalpy convection thickness, $\int_0^\infty \frac{U}{U_e}\left(1 - \frac{H^*}{H_e^*}\right)dY$

Subscripts:

aw evaluated at wall in insulated case

e evaluated outside boundary layer

o evaluated at reference location (stagnation point) outside boundary layer

r evaluated at reference location in boundary layer

t evaluated at transition point

w evaluated at wall

Primed quantities are evaluated at the temperature T'. A bar over a quantity represents evaluation in the transformed plane; for example, $\overline{c}_f$, $\overline{q}_w$, $\overline{\tau}_w$. A bar under a quantity means it has been made dimensionless with respect to the corresponding quantity at the constant reference location or to a reference value. Thus, $\underline{U}_e \equiv \frac{U_e}{\sqrt{2h_o}}$, $\underline{\rho}_e \equiv \frac{\rho_e}{\rho_o}$, $\underline{r} \equiv \frac{r}{l}$, $\underline{\mu}_r \equiv \frac{\mu_r}{\mu_o}$, and so forth.

THEORY

Derivation of the Transformed Equations

The equations of motion and energy in the physical plane.- The boundary-layer equations of motion and energy may be integrated across the boundary layer to obtain the classical Karman momentum integral and its energy counterpart. See, for example, references 5 and 7. The resulting equations are for axisymmetric steady flow:

Momentum:

$$\frac{d\theta}{dx} + \left[\left(2 + \frac{\delta^*}{\theta}\right)\frac{1}{u_e}\frac{du_e}{dx} + \frac{1}{\rho_e}\frac{d\rho_e}{dx} + \frac{1}{r}\frac{dr}{dx}\right]\theta = \frac{c_f}{2} \tag{1}$$

Energy:

$$\frac{d\varphi}{dx} + \left(\frac{1}{\rho_e}\frac{d\rho_e}{dx} + \frac{1}{u_e}\frac{du_e}{dx} + \frac{1}{H_e^*}\frac{dH_e^*}{dx} + \frac{1}{r}\frac{dr}{dx}\right)\varphi = \frac{-q_w}{\rho_e u_e H_e^*} \tag{2}$$

where

$$\theta \equiv \int_0^\infty \frac{\rho u}{\rho_e u_e}\left(1 - \frac{u}{u_e}\right)dy \tag{3a}$$

$$\delta^* \equiv \int_0^\infty \left(1 - \frac{\rho u}{\rho_e u_e}\right)dy \tag{3b}$$

$$\varphi \equiv \int_0^\infty \frac{\rho u}{\rho_e u_e}\left(1 - \frac{H}{H_e^*}\right)dy \tag{3c}$$

Equations (1) and (2) are very general within the usual Prandtl boundary-layer assumptions requiring that the boundary-layer thickness be small compared with the body radius r and that the fluid be composed of a single constituent gas of arbitrary properties. Air may be assumed to fulfill the last-named requirement if the concentration of its constituents are fixed (no dissociation).

The momentum and energy equations have been solved for many cases of laminar flows. Insufficient knowledge of the form of the turbulent shear, heat transfer, and boundary-layer profiles has made analytic solutions of these equations impossible for turbulent flow. With the aid of certain empirical relations, however, approximate solutions to the momentum equation have been obtained. (See, for example, refs. 1, 3, and 5.) From these solutions it is possible to obtain local friction and heat-transfer coefficients, the latter being computed through use of the Reynolds analogy $N_{St} = \frac{c_f}{2}$ which is valid for zero-pressure-gradient flow with unit Prandtl number and constant wall temperature. For a nonunit Prandtl number, the relation if altered to the form $N_{St} = f\left(N_{Pr}\right)\frac{c_f}{2}$. This problem has been treated most recently in reference 11.

A generalized relation between heat transfer and skin friction, hereafter called the modified Reynolds analogy, may be obtained by combination of equations (1) and (2) with the result

$$-\frac{q_w}{\rho_e u_e H_e^*} = \frac{\varphi}{\theta}\frac{c_f}{2} + \frac{\theta}{H_e^*}\frac{d\left(H_e^* \frac{\varphi}{\theta}\right)}{dx} - \varphi\left(1 + \frac{\delta^*}{\theta}\right)\frac{1}{u_e}\frac{du_e}{dx} \qquad (4)$$

A similar modified Reynolds analogy was first derived in reference 6 and has been used in references 4 and 7. Equation (4) reduces to the conventional Reynolds analogy for zero pressure gradient with an isothermal wall and N_{Pr} equal to 1.

Application of the Stewartson transformation.- Mager has shown (ref. 12) that the Stewartson transformation can be applied to turbulent flow with unit Prandtl number and zero heat transfer in order to reduce the equation of motion to its incompressible form. Where the Prandtl number differs from 1 and heat transfer is permitted, the transformation reduces the momentum equation to a form close to but differing from that for incompressible flow. In the present analysis, a modified form of the Stewartson transformation is applied to the momentum equation and the modified Reynolds analogy relation.

The transformation used herein is given by the following relations:

$$X(x) \equiv \int_0^x \frac{\rho_r \mu_r}{\rho_o \mu_o}\left(\frac{h_e}{h_o}\right)^{1/2} dx \qquad (5)$$

$$Y(x,y) \equiv \left(\frac{h_e}{h_o}\right)^{1/2} \int_0^y \frac{\rho}{\rho_o}\, dy \qquad (6)$$

$$U \equiv \left(\frac{h_o}{h_e}\right)^{1/2} u \qquad (7)$$

The subscript r refers to conditions at some local reference within the boundary layer. The subscript o refers to conditions at some arbitrary reference location outside the boundary layer. Also,

$$\rho_r \mu_r = f(x)$$

$$\rho_o \mu_o = \text{Constant}$$

From the definition of the thickness functions (θ and φ) and the relation between the transformed and physical normal coordinate (eq. (6)) the following relations may be obtained:

$$\theta = \frac{\rho_o}{\rho_e}\left(\frac{h_o}{h_e}\right)^{1/2}\bar{\theta} \tag{8}$$

$$\varphi = \frac{\rho_o}{\rho_e}\left(\frac{h_o}{h_e}\right)^{1/2}\bar{\varphi} \tag{9}$$

where

$$\bar{\theta} \equiv \int_0^\infty \frac{U}{U_e}\left(1 - \frac{U}{U_e}\right)dY = \Delta_U \int_0^1 \frac{U}{U_e}\left(1 - \frac{U}{U_e}\right)d\left(\frac{Y}{\Delta_U}\right) \tag{10a}$$

$$\bar{\varphi} \equiv \int_0^\infty \frac{U}{U_e}\left(1 - \frac{H^*}{H_e{}^*}\right)dY = \Delta_H \int_0^1 \frac{U}{U_e}\left(1 - \frac{H^*}{H_e{}^*}\right)d\left(\frac{Y}{\Delta_H}\right) \tag{10b}$$

$$\Delta_U \equiv \left(\frac{h_e}{h_o}\right)^{1/2}\int_0^{\delta_u} \frac{\rho}{\rho_o}\,dy = (Y)_{U=U_e} \tag{10c}$$

$$\Delta_H \equiv \left(\frac{h_e}{h_o}\right)^{1/2}\int_0^{\delta_H} \frac{\rho}{\rho_o}\,dy = (Y)_{H=H_e} \tag{10d}$$

In a like manner, the displacement thickness δ^* is written as

$$\delta^* = \frac{\rho_o}{\rho_e}\left(\frac{h_o}{h_e}\right)^{1/2}\left[\bar{\delta}_1 - \int_0^\infty \left(1 - \frac{\rho_e}{\rho}\right)dY\right] \tag{11}$$

where

$$\bar{\delta}_1 \equiv \int_0^\infty \left(1 - \frac{U}{U_e}\right)dY \tag{11a}$$

In order to account approximately for the effects of variable specific heats, the following linear relation between density and enthalpy is assumed to be valid:

$$1 - \frac{\rho_e}{\rho} = \alpha\left(1 - \frac{h}{h_e}\right) \tag{12}$$

where α is a constant adjusted so that equation (12) is exact at the wall. Fay and Riddell (ref. 13) used a correlation formula similar to equation (12) but including, in addition, a term in $\left(1 - \frac{h}{h_e}\right)^4$. The coefficient of this added term was small compared with α, and that term is herein neglected.

Combination of equations (8), (11), (12), and the definition of total enthalpy

$$H(x,y) = h(x,y) + \frac{\left[u(x,y)\right]^2}{2} \tag{13}$$

yields

$$\delta^* = \frac{\rho_o}{\rho_e}\left(\frac{h_o}{h_e}\right)^{1/2}\left[\bar{\delta}_1 - \alpha \frac{H_e^*}{h_e}\bar{\delta}_2 + \alpha \frac{u_e^2}{2h_e}\left(\bar{\delta}_1 + \bar{\theta}\right)\right] \tag{14a}$$

$$\frac{\delta^*}{\theta} = \frac{\bar{\delta}_1}{\bar{\theta}}\left(1 + \alpha \frac{u_e^2}{2h_e}\right) - \alpha \frac{H_e^*}{h_e}\frac{\bar{\delta}_2}{\bar{\theta}} + \alpha \frac{u_e^2}{2h_e} \tag{14b}$$

where

$$\bar{\delta}_2 \equiv \int_0^\infty \left(1 - \frac{H^*}{H_e^*}\right)dY = \Delta_H \int_0^1 \left(1 - \frac{H^*}{H_e^*}\right)d\left(\frac{Y}{\Delta_H}\right) \tag{14c}$$

The momentum equation (eq. (1)) and the modified Reynolds analogy (eq. (4)) may be transformed to the Stewartson plan through the use of equations (5) to (14). If the energy equation outside the boundary layer is

$$h_e(x) + \frac{\left[u_e(x)\right]^2}{2} = H_e = \text{Constant} \tag{15}$$

the momentum equation is

$$\frac{d\bar{\theta}}{dX} + \left\{\left[2 + \frac{\bar{\delta}_1}{\bar{\theta}} + \frac{u_e^2}{2H_e}(\alpha - 1)\left(1 + \frac{\bar{\delta}_1}{\bar{\theta}}\right) - \alpha \frac{H_e^*}{H_e}\frac{\bar{\delta}_2}{\bar{\theta}}\right]\frac{1}{U_e}\frac{dU_e}{dX} + \frac{1}{r}\frac{dr}{dX}\right\}\bar{\theta} =$$

$$\frac{c_f}{2}\frac{\rho_o \mu_o}{\rho_r \mu_r}\frac{\rho_e}{\rho_o} \tag{16}$$

and the modified Reynolds analogy is

$$-\frac{q_w}{\rho_e u_e H_e^*}\frac{\rho_e}{\rho_o}\frac{\rho_o\mu_o}{\rho_r\mu_r} = \frac{\bar{\varphi}}{\bar{\theta}}\frac{c_f}{2}\frac{\rho_o\mu_o}{\rho_r\mu_r}\frac{\rho_e}{\rho_o} + \bar{\varphi}\left\{\frac{1}{H_e^*}\frac{dH_e^*}{dX} + \frac{1}{\bar{\varphi}/\bar{\theta}}\frac{d(\bar{\varphi}/\bar{\theta})}{dX} - \left[1 + \frac{\bar{\delta}_1}{\bar{\theta}} + \frac{u_e^2}{2H_e}(\alpha - 1)\left(1 + \frac{\bar{\delta}_1}{\bar{\theta}}\right) - \alpha\frac{H_e^*}{H_e}\frac{\bar{\delta}_2}{\bar{\theta}}\right]\frac{1}{U_e}\frac{dU_e}{dX}\right\} \tag{17}$$

Equation (16) takes on a form almost like the incompressible form with the definition of the transformed friction coefficient $\bar{c}_f$ as

$$\frac{\bar{c}_f}{2} \equiv \frac{c_f}{2}\frac{\rho_o\mu_o}{\rho_r\mu_r}\frac{\rho_e}{\rho_o} \tag{18}$$

The transformed friction coefficient is related to the transformed wall shear $\bar{\tau}_w$ by the definition

$$\frac{\bar{c}_f}{2} \equiv \frac{\bar{\tau}_w}{\rho_o U_e^2} \tag{19}$$

Combination of equations (18), (19), (6), and the definition of the friction coefficient in the physical plane $\left(c_f/2 \equiv \tau_w/\rho_e u_e^2\right)$ yields the following relation between wall shears

$$\bar{\tau}_w = \frac{\rho_o\mu_o}{\rho_r\mu_r}\frac{h_o}{h_e}\tau_w \tag{20}$$

In an analogous manner, the transformed heat-transfer coefficient is defined as

$$\frac{\bar{q}_w}{\rho_o U_e H_e^*} \equiv \frac{q_w}{\rho_e u_e H_e^*}\frac{\rho_e}{\rho_o}\frac{\rho_o\mu_o}{\rho_r\mu_r} \tag{21}$$

The heat transfers in the two systems are related by

$$\bar{q}_w = \frac{\rho_o\mu_o}{\rho_r\mu_r}\left(\frac{h_o}{h_e}\right)^{1/2} q_w \tag{22}$$

Substitution of definitions (18) and (21) into the transformed momentum equation and modified Reynolds analogy (eqs. (16) and (17)), respectively) reduces these relations to their final general form.

The momentum equation is

$$\frac{d\bar{\theta}}{dX} + \left\{\left[2 + \frac{\bar{\delta}_1}{\bar{\theta}} + \frac{u_e^2}{2H_e}(\alpha - 1)\left(1 + \frac{\bar{\delta}_1}{\bar{\theta}}\right) - \alpha \frac{H_e^*}{H_e} \frac{\bar{\delta}_2}{\bar{\theta}}\right]\frac{1}{U_e}\frac{dU_e}{dX} + \frac{1}{r}\frac{dr}{dX}\right\}\bar{\theta} = \frac{\bar{c}_f}{2} \tag{23}$$

and the modified Reynolds analogy is

$$-\frac{\bar{q}_w}{\rho_o U_e H_e^*} = \frac{\bar{\varphi}}{\bar{\theta}}\frac{\bar{c}_f}{2} + \bar{\varphi}\left\{\frac{1}{H_e^*}\frac{dH_e^*}{dX} + \frac{1}{\bar{\varphi}/\bar{\theta}}\frac{d(\bar{\varphi}/\bar{\theta})}{dX} - \left[1 + \frac{\bar{\delta}_1}{\bar{\theta}} + \frac{u_e^2}{2H_e}\left(1 + \frac{\bar{\delta}_1}{\bar{\theta}}\right)(\alpha - 1) - \alpha \frac{H_e^*}{H_e}\frac{\bar{\delta}_2}{\bar{\theta}}\right]\frac{1}{U_e}\frac{dU_e}{dX}\right\} \tag{24}$$

Equation (23), even for constant specific heat ($\alpha = 1$), is not in general equivalent to the incompressible momentum equation because of the presence of the term $\left(-\alpha \frac{\bar{\delta}_2}{\bar{\theta}} \frac{H_e^*}{H_e} \frac{1}{U_e} \frac{dU_e}{dX}\right)$. For unit Prandtl number with zero heat transfer, H_e^* vanishes; thus, the coefficient of the velocity gradient term would take on its incompressible form $2 + \frac{\bar{\delta}_1}{\bar{\theta}}$ in that case.

The present analysis for axisymmetric flows can be specialized to the two-dimensional case by considering r as a constant and $dr/dx = 0$; thus, r is eliminated from the momentum equation.

Relation between total enthalpy and velocity profiles.- In order to solve the system of equations outlined in the preceding section, it is necessary to specify velocity and total enthalpy profiles and a friction law, but it is desirable to investigate first a relation between total enthalpy and velocity profiles which should have rather general significance.

For the special case of zero pressure gradient, unit Prandtl number, and an isothermal wall, the Crocco relation between total enthalpy and velocity is valid. This equation is

$$H = a + bu$$

Boundary conditions at the wall and stream give the specific relation

$$\frac{H^*}{H_e^*} = \frac{u}{u_e}$$

Pressure gradient, nonunit Prandtl number, and nonisothermal wall will each probably alter this relation. In reference 11, for example, with the assumption of nonunit Prandtl number in the laminar sublayer, the total enthalpy is found to be a quadratic function of velocity in the sublayer.

Dennison assumed the validity of the quadratic relation

$$H = a + bu + cu^2 \tag{25}$$

for the case with nonzero pressure gradient but with unit Prandtl number and isothermal wall. The coefficients of the velocity terms were found to be functions of the local pressure gradient and the heat transfer was evaluated from the skin friction by using a relation analogous to the modified Reynolds analogy of the present report. A multiplication factor was then suggested to account for nonunit Prandtl number.

Rather than complicate the present analysis by combining the Prandtl number and pressure gradient effects into the enthalpy-velocity relation, the approach of the present report is to follow Dennison in assuming that the Prandtl number is 1 and that equation (25) is valid through the entire boundary layer. The coefficients of the velocity terms in equation (25) are then evaluated as functions of pressure gradient and wall enthalpy. A correction to account for nonunit Prandtl number is later introduced. Boundary conditions for equation (25) were such that at the wall

$$y = Y = 0$$

$$u = U = 0$$

$$H = H_w$$

and at the outer edge of the boundary layer

$$y = \delta$$

$$Y = \Delta$$

$$u = u_e$$

$$U = U_e$$

$$H = H_e$$

The form of equation (25) and the second boundary condition require equal velocity and enthalpy thicknesses, that is, $\delta_u = \delta_H = \delta$ and $\Delta_U = \Delta_H = \Delta$. This restriction is not serious since a unit Prandtl number has already been assumed; thus equal or nearly equal thicknesses are implied. Application of the boundary conditions to equation (25) yields

$$\frac{H^*}{H_e^*} = \frac{u}{u_e}\left(1 - c\,\frac{u_e^2}{H_e^*}\right) + c\,\frac{u_e^2}{H_e^*}\left(\frac{u}{u_e}\right)^2 \tag{26a}$$

$$\frac{H^*}{H_e^*} = \frac{U}{U_e}\left(1 - c\,\frac{u_e^2}{H_e^*}\right) + c\,\frac{u_e^2}{H_e^*}\left(\frac{U}{U_e}\right)^2 \tag{26b}$$

Equations (26) are assumed to be valid independent of the type of velocity profiles and the friction law describing the flow. A qualitative check of their validity may be obtained by comparison with laminar-flow results. Plotted in figure 1 are results of the similar solutions of reference 14 for zero and favorable pressure gradients and cooled walls. The quantity β of reference 14 is a pressure gradient parameter which is zero for zero pressure gradient and increasingly positive for increasingly favorable pressure gradients. Plotted also is equation (26a) for various values of $c\,\frac{u_e^2}{H_e^*}$ from 0 to 1.0, values which also represent zero and favorable pressure gradients and cooled walls. The quantities β and $c\,\frac{u_e^2}{H_e^*}$ are not simply related to one another and the present comparison is intended as only a qualitative one. With this qualification the two sets of curves in figure 1 show sufficient resemblance in shape to lend support to the present approach.

With the aid of equation (26b) the thickness functions $\bar{\delta}_2$ and $\bar{\varphi}$ may be expressed in terms of integrals of velocity functions as follows:

$$\bar{\delta}_2 \equiv \Delta \int_0^1 \left(1 - \frac{H^*}{H_e^*}\right) d\left(\frac{Y}{\Delta}\right) = \bar{\delta}_1 + c\,\frac{u_e^2}{H_e^*}\,\bar{\theta} \tag{27}$$

$$\bar{\varphi} \equiv \Delta \int_0^1 \frac{U}{U_e}\left(1 - \frac{H^*}{H_e^*}\right) d\left(\frac{Y}{\Delta}\right) = \bar{\theta} + c\,\frac{u_e^2}{H_e^*}\,\bar{\lambda} \tag{28}$$

where

$$\bar{\lambda} \equiv \Delta \int_0^1 \left(\frac{U}{U_e}\right)^2 \left(1 - \frac{U}{U_e}\right) d\left(\frac{Y}{\Delta}\right) \tag{29}$$

Definition of Z as

$$Z \equiv c \frac{u_e^2}{H_e^*} \frac{\bar{\lambda}}{\bar{\theta}}$$

yields the relations

$$\frac{\bar{\delta}_2}{\bar{\theta}} = \frac{\bar{\delta}_1}{\bar{\theta}} + Z \frac{\bar{\theta}}{\bar{\lambda}} \tag{30}$$

$$\bar{\varphi}/\bar{\theta} = 1 + Z \tag{31}$$

One more equation is needed to complete the formulation of the problem. Equation (24) represents the relation between heat transfer and skin friction in the transformed plane. Another relation between the same two quantities, one which must be compatible with equation (24), may be derived from equation (26b) as follows:

Consider the derivative of enthalpy with respect to velocity from equation (26b) evaluated at the wall. This relation is

$$\left(\frac{dH}{dU}\right)_{Y=0} = \frac{H_e^*}{U_e}\left(1 - Z \frac{\bar{\theta}}{\bar{\lambda}}\right) \tag{32}$$

The shear and heat transfer at the wall can, in general, be written respectively, as

$$\bar{\tau}_w = \mu\left(\frac{\partial U}{\partial Y}\right)_{Y=0} \tag{33a}$$

$$\bar{q}_w = -k\left(\frac{\partial T}{\partial Y}\right)_{Y=0} = -\frac{k}{c_p}\left(\frac{\partial H}{\partial Y}\right)_{Y=0} \tag{33b}$$

because the apparent turbulent shear and heat transfer vanish at the wall. The values of μ, k, and c_p are not here specified but apply to a common location. The ratio of shear to heat transfer is easily obtained from equations (33) as

$$\frac{\bar{\tau}_w}{\bar{q}_w} = - \frac{\mu c_p}{k} \left(\frac{dU}{dH}\right)_{Y=0}$$

and, since the Prandtl number has been assumed to be equal to 1,

$$\frac{- \dfrac{\bar{q}_w}{\rho_o U_e H_e^*}}{\dfrac{\bar{\tau}_w}{\rho_o U_e^2}} = \frac{U_e}{H_e^*} \left(\frac{dH}{dU}\right)_{Y=0} \tag{34}$$

Combining equations (32) and (34) yields

$$- \frac{\bar{q}_w}{\rho_o U_e H_e^*} = \left(1 - Z \frac{\bar{\theta}}{\bar{\lambda}}\right) \frac{\bar{c}_f}{2} \tag{35}$$

Equations (24) and (35), each a form of the modified Reynolds analogy, are assumed to be equivalent. A differential equation for Z results from this assumption. After substitution of equations (30) and (31) into the result, the following equation is obtained

$$\frac{dZ}{dX} + Z \left[\frac{1}{\bar{\theta}} \frac{\bar{c}_f}{2} \left(1 + \frac{\bar{\theta}}{\bar{\lambda}}\right) + \frac{1}{H_e^*} \frac{dH_e^*}{dX} - \left(\Gamma - 1 - \alpha \frac{H_e^*}{H_e} \frac{\bar{\theta}}{\bar{\lambda}}\right) \frac{1}{U_e} \frac{dU_e}{dX} \right] +$$

$$\frac{1}{H_e^*} \frac{dH_e^*}{dX} - \frac{\Lambda}{U_e} \frac{dU_e}{dX} = 0 \tag{36}$$

where

$$\Gamma \equiv 2 + \frac{H_w}{H_e} \frac{\bar{\delta}_1}{\bar{\theta}} + (\alpha - 1) \left[\frac{u_e^2}{2H_e} \left(1 + \frac{\bar{\delta}_1}{\bar{\theta}}\right) - \frac{H_e^*}{H_e} \frac{\bar{\delta}_1}{\bar{\theta}} \right] - \alpha \frac{H_e^*}{H_e} Z \frac{\bar{\theta}}{\bar{\lambda}} \tag{37a}$$

$$\Lambda \equiv \Gamma - 1 + \alpha \frac{H_e^*}{H_e} Z \frac{\bar{\theta}}{\bar{\lambda}} = 1 + \frac{H_w}{H_e} \frac{\bar{\delta}_1}{\bar{\theta}} + (\alpha - 1) \left[\frac{u_e^2}{2H_e} \left(1 + \frac{\bar{\delta}_1}{\bar{\theta}}\right) - \frac{H_e^*}{H_e} \frac{\bar{\delta}_1}{\bar{\theta}} \right] \tag{37b}$$

Note that Γ is a function of Z but that Λ is not. Finally, by using equation (30) the momentum equation (23) is rewritten as

$$\frac{d\bar{\theta}}{dX} + \left(\frac{\Gamma}{U_e}\frac{dU_e}{dX} + \frac{1}{r}\frac{dr}{dX}\right)\bar{\theta} = \frac{\bar{c}_f}{2} \tag{38}$$

Equations (36) and (38) form a pair of simultaneous nonlinear differential equations of the first order. The boundary conditions chosen are those resulting from the simple assumption of instantaneous transition from laminar to fully developed turbulent flow; that is, $\bar{\theta} = \bar{\theta}_t$, $Z = Z_t$ at $X = X_t$.

The special case of constant specific heats yields the simpler equations

$$\Gamma = 2 + \frac{H_w}{H_e}\frac{\bar{\delta}_1}{\bar{\theta}} - \frac{H_e^*}{H_e} Z \frac{\bar{\theta}}{\bar{\lambda}} \tag{39a}$$

$$\Lambda = 1 + \frac{H_w}{H_e}\frac{\bar{\delta}_1}{\bar{\theta}} \tag{39b}$$

The terms in $\frac{1}{H_e^*}\frac{dH_e^*}{dX}$ have been retained in equation (36) in order that the restriction to isothermal walls may be relaxed to include $H_w = H_w(x)$. The assumption is made that the gross effects of a non-isothermal wall are accounted for in this equation without the necessity of further modifying the enthalpy-velocity relation (26a) or the dependent relation between $\bar{q}_w$ and $\bar{c}_f$ (eq. (35)).

Application of a Simple Velocity Profile and Friction Law

Assumption of power velocity profile and friction law.- In the absence of detailed knowledge of the turbulent velocity profiles and friction law for compressible flow about a body of revolution with streamwise pressure gradient, certain assumptions are made. These are:

(1) The effect of compressibility is completely accounted for by the Stewartson transformation; thus, incompressible flow relations may be assumed to be valid in the transformed plane.

(2) The effect of pressure gradient upon the velocity profile and friction law is negligible; thus, zero-pressure-gradient relations may be used. The incompressible, zero-pressure-gradient relations chosen for the present analysis are

$$\frac{U}{U_e} = \left(\frac{Y}{\Delta}\right)^{1/n} \tag{40}$$

$$\frac{\bar{c}_f}{2} = A_m \left(\frac{\rho_o U_e \bar{\theta}}{\mu_o}\right)^{-1/m} \tag{41}$$

where A_m is assumed to be constant. Velocity profiles of the form of equation (40) have been observed in flows with pressure gradient. (See ref. 15.) The Ludwieg-Tillman friction law of this reference is of the form of equation (41) but with A_m as a function of shape factor. Since the shape factor is not altered seriously by favorable pressure gradients but is a strong function of adverse pressure gradients, the present analysis is limited to favorable and weak adverse pressure gradients.

(3) The velocity profile and friction law (eqs. (40) and (41), respectively) are unaffected by the curvature in the axially symmetric case so that these two-dimensional relations may be assumed to be valid. With the assumption that the boundary-layer thickness is small compared with the body radius, the local curvature due to the axial symmetry would be expected to have a small influence upon the local friction law because, locally, the turbulent exchange should far outweigh the momentum change caused by the varying cross-sectional area. On these physical grounds the assumption of no effect of body radius upon profiles and shear law seems to be justified. Some methematical justification might be seen from the following: If a turbulent analog to the laminar Mangler transformation were employed, equations (40) and (41) would be assumed to be valid in the resulting two-dimensional flow. It can be shown that such a procedure leads to an expression for the physical (three-dimensional) friction coefficient equivalent to that obtained by the present method, that is, the expression which results from combination of equations (5), (6), (18), and (41),

$$\frac{c_f}{2} = A_m \frac{\rho_r \mu_r}{\rho_o \mu_o} \frac{\rho_o}{\rho_e} \left(\frac{\mu_o}{\mu_e}\right)^{1/m} \left(\frac{\rho_e u_e \theta}{\mu_e}\right)^{-1/m} \tag{42}$$

Thickness functions.- For the velocity profile of equation (40), the thickness functions of equations (10a), (11a), and (29) may be evaluated

$$\left.\begin{aligned}
\frac{\overline{\delta}_1}{\Delta} &= \frac{1}{n+1} \\
\frac{\overline{\theta}}{\Delta} &= \frac{n}{(n+1)(n+2)} \\
\frac{\overline{\lambda}}{\Delta} &= \frac{n}{(n+2)(n+3)} \\
\frac{\overline{\delta}_1}{\overline{\theta}} &= \frac{n+2}{n} \\
\frac{\overline{\theta}}{\overline{\lambda}} &= \frac{n+3}{n+1}
\end{aligned}\right\} \tag{43}$$

Differential equations.- Equation (41) is substituted into the momentum equation (38) and, after some rearranging, the result is

$$\frac{d(\overline{\theta})^{\frac{m+1}{m}}}{dX} + \left(\frac{m+1}{m}\right)\left(\frac{\Gamma}{U_e}\frac{dU_e}{dX} + \frac{1}{r}\frac{dr}{dX}\right)(\overline{\theta})^{\frac{m+1}{m}} = A_m\left(\frac{m+1}{m}\right)\left(\frac{\rho_o U_e}{\mu_o}\right)^{-\frac{1}{m}} \tag{44}$$

The modified Reynolds analogy equation (36) becomes

$$\frac{dZ}{dX} + Z\left[A_m\left(\frac{\rho_o U_e}{\mu_o}\right)^{-\frac{1}{m}}(\overline{\theta})^{-\frac{m+1}{m}}\left(1 + \frac{\overline{\theta}}{\overline{\lambda}}\right) + \frac{1}{H_e^*}\frac{dH_e^*}{dX} - \left(\Gamma - 1 - \alpha\frac{H_e^*}{H_e}\frac{\overline{\theta}}{\overline{\lambda}}\right)\frac{1}{U_e}\frac{dU_e}{dX}\right] + \frac{1}{H_e^*}\frac{dH_e^*}{dX} - \frac{\Lambda}{U_e}\frac{dU_e}{dX} = 0 \tag{45}$$

The dependent variables are now $(\overline{\theta})^{\frac{m+1}{m}}$ and Z.

Nondimensionalization.- Equations (44) and (45) may be made dimensionless with respect to the constant reference conditions p_o, ρ_o, μ_o, h_o, and a constant reference length l. Dimensionless quantities are then, for example,

$$\underline{U}_e \equiv \frac{U_e}{\sqrt{2h_o}} \qquad \underline{\rho}_e \equiv \frac{\rho_e}{\rho_o} \qquad \underline{\mu}_r \equiv \frac{\mu_r}{\mu_o}$$

$$\underline{h}_e \equiv \frac{h_e}{h_o} \qquad \underline{r} \equiv \frac{r}{l} \qquad \underline{x} \equiv \frac{x}{l}$$

$$\xi \equiv \frac{X}{l} = \int_0^{\underline{x}} \underline{\rho}_r \underline{\mu}_r \left(\underline{h}_e\right)^{1/2} d\underline{x}$$

Equations (44) and (45) become

$$\frac{d\Theta}{d\xi} + \left(\frac{m+1}{m}\right)\left(\frac{\Gamma}{\underline{U}_e}\frac{d\underline{U}_e}{d\xi} + \frac{1}{\underline{r}}\frac{d\underline{r}}{d\xi}\right)\Theta = A_m\left(\frac{m+1}{m}\right)\left(\underline{U}_e\right)^{-\frac{1}{m}} \tag{46}$$

$$\frac{dZ}{d\xi} + Z\left[\frac{A_m\left(\underline{U}_e\right)^{-\frac{1}{m}}}{\Theta}\left(1 + \frac{\bar{\theta}}{\bar{\lambda}}\right) + \frac{1}{H_e^*}\frac{dH_e^*}{d\xi} - \left(\Gamma - 1 - \alpha\frac{H_e^*}{H_e}\frac{\bar{\theta}}{\bar{\lambda}}\right)\frac{1}{\underline{U}_e}\frac{d\underline{U}_e}{d\xi}\right] +$$

$$\frac{1}{H_e^*}\frac{dH_e^*}{d\xi} - \frac{\Lambda}{\underline{U}_e}\frac{d\underline{U}_e}{d\xi} = 0 \tag{47}$$

where

$$\Theta \equiv \left(\frac{\bar{\theta}}{l}\right)^{\frac{m+1}{m}}\left(N_{Ro}\right)^{\frac{1}{m}} \tag{48a}$$

$$N_{Ro} \equiv \frac{\rho_o\sqrt{2h_o}\,l}{\mu_o} \tag{48b}$$

The quantity Θ is a "reduced" momentum thickness, and the Reynolds number dependence of the equations is implicit in its definition and the Reynolds number enters these equations in no other way. Equations (46) and (47) are nonlinear differential equations through the dependence of the quantity Γ upon the dependent variable Z. Step-by-step numerical solution is required and the solution is hereafter termed the "exact" solution.

Evaluation of Skin Friction and Heat Transfer

When the momentum thickness parameter Θ and the factor Z have been computed, the skin friction and heat transfer may be obtained as follows: Combination of equations (41) and (48) gives

$$\frac{\bar{c}_f}{2}\left(N_{Ro}\right)^{\frac{1}{m+1}} = A_m\left(\underline{U}_e\right)^{-\frac{1}{m}}(\Theta)^{-\frac{1}{m+1}} \tag{49}$$

In the physical plane, from equations (18) and (49),

$$\frac{c_f}{2}\left(N_{Ro}\right)^{\frac{1}{m+1}} = A_m\left(\underline{U}_e\right)^{-\frac{1}{m}}(\Theta)^{-\frac{1}{m+1}}\frac{\underline{\rho}_r\underline{\mu}_r}{\underline{\rho}_e} \tag{50}$$

Then, for unit Prandtl number, from equations (21) and (35)

$$-\frac{q_w}{\rho_e u_e H_e^*}\left(N_{Ro}\right)^{\frac{1}{m+1}} = \left(1 - Z\frac{\bar{\theta}}{\bar{\lambda}}\right)\frac{\underline{\rho}_r\underline{\mu}_r}{\underline{\rho}_e}\left[\frac{\bar{c}_f}{2}\left(N_{Ro}\right)^{\frac{1}{m+1}}\right] \tag{51}$$

For Prandtl number other than one, the enthalpy driving potential for heat transfer is $H_{aw} - H_w$, and this substitution for H_e^* in equation (51), along with the empirical Prandtl number correction, gives the result

$$N_{St}\left(N_{Ro}\right)^{\frac{1}{m+1}} = \left(1 - Z\frac{\bar{\theta}}{\bar{\lambda}}\right)\left(N_{Pr}\right)^{-2/3}\frac{\underline{\rho}_r\underline{\mu}_r}{\underline{\rho}_e}\left[\frac{\bar{c}_f}{2}\left(N_{Ro}\right)^{\frac{1}{m+1}}\right]$$

$$= \left(1 - Z\frac{\bar{\theta}}{\bar{\lambda}}\right)\left(N_{Pr}\right)^{-2/3}\left[\frac{c_f}{2}\left(N_{Ro}\right)^{\frac{1}{m+1}}\right] \tag{52}$$

where

$$N_{St} \equiv \frac{-q_w}{\rho_e u_e H_{aw}^*}$$

Special Cases

Solution for H_e^* equal zero.- For the case H_e^* equal to zero with arbitrary pressure gradient and constant specific heats, equations (46) and (47) may be solved in closed form. The term $\frac{1}{H_e^*}\frac{dH_e^*}{d\xi}$

in equation (47) appears to be indeterminate but may be seen to be zero since for any constant value $H_w \neq H_e$ this term is identically zero regardless of how small the difference $H_e - H_w \equiv H_e^*$ is allowed to become.

The differential equations describing this flow are, from equations (37), (46), and (47),

$$\frac{d\Theta}{d\xi} + \left(\frac{m+1}{m}\right)\left(\frac{\Gamma}{\underline{U}_e}\frac{d\underline{U}_e}{d\xi} + \frac{1}{\underline{r}}\frac{d\underline{r}}{d\xi}\right)\Theta = A_m\left(\frac{m+1}{m}\right)\left(\underline{U}_e\right)^{-\frac{1}{m}} \tag{53}$$

$$\frac{dZ}{d\xi} + Z\left[\frac{A_m\left(\underline{U}_e\right)^{-\frac{1}{m}}}{\Theta}\left(1 + \frac{\overline{\theta}}{\overline{\lambda}}\right) - \frac{(\Gamma - 1)}{\underline{U}_e}\frac{d\underline{U}_e}{d\xi}\right] = \frac{\Lambda}{\underline{U}_e}\frac{d\underline{U}_e}{d\xi} \tag{54}$$

$$\Gamma = 2 + \frac{\overline{\delta}_1}{\overline{\theta}} \tag{55a}$$

$$\Lambda = 1 + \frac{\overline{\delta}_1}{\overline{\theta}} = \Gamma - 1 \tag{55b}$$

The thickness ratios $\frac{\overline{\delta}_1}{\overline{\theta}}$ and $\frac{\overline{\theta}}{\overline{\lambda}}$ were evaluated for power profiles and are given in equations (43). Since n was assumed to be constant, these ratios, Γ, and Λ are then constant, and equations (53) and (54) are linear and may be integrated in closed form. The momentum equation (53) may be written after some manipulation as

$$\frac{d}{d\xi}\left[\Theta\left(\underline{r}\underline{U}_e^{\Gamma}\right)^{\frac{m+1}{m}}\right] = A_m\left(\frac{m+1}{m}\right)\left(\underline{r}\right)^{\frac{m+1}{m}}\left(\underline{U}_e\right)^{\frac{\Gamma(m+1)-1}{m}} \tag{56}$$

Equation (56) is integrated to give

$$\Theta = \Theta_t \frac{\left(\underline{r}\underline{U}_e^{\Gamma}\right)_t^{\frac{m+1}{m}}}{\left(\underline{r}\underline{U}_e^{\Gamma}\right)^{\frac{m+1}{m}}} + A_m\left(\frac{m+1}{m}\right)\left(\underline{U}_e\right)^{-\frac{1}{m}} \frac{\int_{\xi_t}^{\xi} \left(\underline{r}\right)^{\frac{m+1}{m}}\left(\underline{U}_e\right)^{\frac{\Gamma(m+1)-1}{m}} d\xi}{\left(\underline{r}\right)^{\frac{m+1}{m}}\left(\underline{U}_e\right)^{\frac{\Gamma(m+1)-1}{m}}} \tag{57a}$$

In the special case $\Theta_t = \xi_t = 0$,

$$\Theta = A_m\left(\frac{m+1}{m}\right)\left(\underline{U}_e\right)^{-\frac{1}{m}} \frac{\displaystyle\int_0^{\xi} (\underline{r})^{\frac{m+1}{m}} \left(\underline{U}_e\right)^{\frac{\Gamma(m+1)-1}{m}} d\xi}{(\underline{r})^{\frac{m+1}{m}} \left(\underline{U}_e\right)^{\frac{\Gamma(m+1)-1}{m}}} \tag{57b}$$

The modified Reynolds analogy equation (54) is of the form

$$\frac{dZ}{d\xi} + Zf_1(\xi) = \frac{\Lambda}{\underline{U}_e}\frac{d\underline{U}_e}{d\xi}$$

and the solution is

$$Z = e^{-\int f_1(\xi)d\xi}\left[\int e^{\int f_1(\xi)d\xi}\left(\frac{\Lambda}{\underline{U}_e}\frac{d\underline{U}_e}{d\xi}\right)d\xi + K\right] \tag{58}$$

where

$$f_1(\xi) = \frac{A_m\left(\underline{U}_e\right)^{-\frac{1}{m}}}{\Theta}\left(1 + \frac{\overline{\theta}}{\overline{\lambda}}\right) \cdot \frac{\Gamma - 1}{\underline{U}_e}\frac{d\underline{U}_e}{d\xi}$$

In general, the integral $\int f_1(\xi)d\xi$ will have to be evaluated numerically after completion of the solution of the momentum equation. For the special case $\Theta_t = \xi_t = 0$; however, the solution for Θ yields

$$\frac{A_m\left(\underline{U}_e\right)^{-\frac{1}{m}}}{\Theta} = \frac{m}{m+1}\frac{(\underline{r})^{\frac{m+1}{m}}\left(\underline{U}_e\right)^{\frac{\Gamma(m+1)-1}{m}}}{\displaystyle\int_0^{\xi}(\underline{r})^{\frac{m+1}{m}}\left(\underline{U}_e\right)^{\frac{\Gamma(m+1)-1}{m}}d\xi} = \frac{m}{m+1}\frac{d\log_e F}{d\xi}$$

where

$$F = F(\xi) \equiv \int_0^{\xi} (\underline{r})^{\frac{m+1}{m}}\left(\underline{U}_e\right)^{\frac{\Gamma(m+1)-1}{m}} d\xi$$

Then

$$\int f_1(\xi)d\xi = \left(1 + \frac{\overline{\theta}}{\overline{\lambda}}\right)\left(\frac{m}{m+1}\right)\log_e \Gamma - (\Gamma - 1)\log_e \underline{U}_e$$

and

$$e^{\int f_1(\xi)d\xi} = (F)^{\frac{m}{m+1}\left(1+\frac{\bar{\theta}}{\bar{\lambda}}\right)}\left(\underline{U}_e\right)^{-(\Gamma-1)} \tag{59}$$

Equation (59) is substituted into equation (58) and the following equation is obtained:

$$Z = \frac{\left(\underline{U}_e\right)^{\Gamma-1}}{(F)^{\frac{m}{m+1}\left(1+\frac{\bar{\theta}}{\bar{\lambda}}\right)}}\left[\int \frac{(F)^{\frac{m}{m+1}\left(1+\frac{\bar{\theta}}{\bar{\lambda}}\right)}}{\left(\underline{U}_e\right)^{\Gamma-1}}\left(\frac{\Lambda}{\underline{U}_e}\frac{d\underline{U}_e}{d\xi}\right)d\xi + K\right] \tag{60}$$

The constant K must be set equal to zero in order that equation (60) leads to a stagnation-region solution consistent with that developed in the appendix. The limits on the integral are set from zero to ξ, which, in conjunction with $K = 0$, allows Z to approach zero as expected far downstream on a blunted cylinder or cone as $\frac{d\underline{U}_e}{d\xi}$ approaches zero.

The final result is

$$Z = \frac{\left(\underline{U}_e\right)^{\Gamma-1}}{(F)^{\frac{m}{m+1}\left(1+\frac{\bar{\theta}}{\bar{\lambda}}\right)}}\int_0^{\xi} \frac{(F)^{\frac{m}{m+1}\left(1+\frac{\bar{\theta}}{\bar{\lambda}}\right)}}{\left(\underline{U}_e\right)^{\Gamma-1}}\left(\frac{\Lambda}{\underline{U}_e}\frac{d\underline{U}_e}{d\xi}\right)d\xi \tag{61}$$

Equations (57b) and (61) provide explicit solutions to the momentum and modified Reynolds analogy equations for the case $\Theta_t = \xi_t = 0$ for $H_e^* = 0$, which, for unit Prandtl number and recovery factor, corresponds to an insulated wall.

Other special cases.- The special cases of the flat plate, the cone in supersonic flow, and two- and three-dimensional stagnation regions are discussed in the appendix. The stagnation-region solutions have value in establishing initial conditions for the complete solution of equations (46) and (47) when the flow is assumed to be turbulent from the stagnation point. The results for two- and three-dimensional stagnation regions are given in the appendix (eqs. (A10) to (A15)) and plots of the variation of Z_o with the cooling ratio H_w/H_e are shown in figures (2a) and (2b) for $\alpha = 1$, $m = 4$, and $n = 7$. Although the results (eqs. (A10) to (A15)) are also valid for heated walls $H_w/H_e > 1$,

only the cooled-wall results are shown. For stagnation flow, the reduced momentum thickness Θ varies directly with $\xi^{\frac{m-1}{m}}$, or in the physical plane, θ varies directly with $x^{\frac{m-1}{m+1}}$. The momentum thickness at the stagnation point is zero, a consequence of the assumed relation between c_f and θ. The term Z is independent of x in the stagnation region.

Approximate Solution

The special case of flow with pressure gradient but zero enthalpy difference H_e^* was shown to give simple closed-form solutions for $\Theta_t = \xi_t = 0$ and constant specific heats. (See eqs. (57b) and (61).) An approximate method for the general case based on this special case is now developed.

The nonlinearity of equations (46) and (47) is caused by the dependence of Γ upon Z. (See eq. (37a).) Figure 3 shows plots of the variation of Γ with cooling ratio H_w/H_e for various values of Z with $\alpha = 1$ and $n = 7$. The upper limit of Z of 0.8 was chosen since, for this value, the Stanton number is zero for a finite friction coefficient. (See eq. (52).) A value of Z in excess of this maximum would imply heat transfer in a direction opposite to that of the heat-transfer potential H_{aw}^*, a behavior not expected on physical grounds except perhaps where H_{aw}^* passes through zero. Figure 3 shows that Γ is not a strong function of Z for given H_w/H_e. For H_w/H_e approaching zero, the dependence is a maximum; for unit H_w/H_e, the dependence disappears. Similar behavior would occur for hot walls $\left(H_w/H_e > 1.0\right)$ and nonunit α is not expected to alter this dependence seriously.

The approximation assumes that Γ is given by equation (37a) specialized for an average value of Z equal to 0.4. Thus,

$$(\Gamma)_{Z=0.4} \equiv \bar{\Gamma} = 2 + \frac{H_w}{H_e}\frac{\bar{\delta}_1}{\bar{\theta}} + (\alpha - 1)\left[\frac{u_e^2}{2H_e}\left(1 + \frac{\bar{\delta}_1}{\bar{\theta}}\right) - \frac{H_e^*}{H_e}\frac{\bar{\delta}_1}{\bar{\theta}}\right] - 0.4\alpha\frac{H_e^*}{H_e}\frac{\bar{\theta}}{\bar{\lambda}} \tag{62}$$

Equation (62) is assumed to be correct for an arbitrary value of n. The momentum equation (46) is linear with $\bar{\Gamma}$ substituted for Γ and may be integrated upon the neglect of $\frac{d\bar{\Gamma}}{d\xi}$ with respect to $\frac{dU_e}{d\xi}$. The

derivative $\frac{d\bar{\Gamma}}{d\xi}$ is seen to depend upon $\frac{d(H_w/H_e)}{d\xi}$ and $\frac{d\alpha}{d\xi}$, both of which are assumed to be small. Because $\frac{dU_e}{d\xi}$ approaches zero downstream on blunted cylinders or cones, the approximation may fail in these regions. However, with this assumption and some manipulation, equation (46) is rewritten as

$$\frac{d}{d\xi}\left[\Theta\left(\underline{r}\underline{U}_e\bar{\Gamma}\right)^{\frac{m+1}{m}}\right] = A_m\left(\frac{m+1}{m}\right)(\underline{r})^{\frac{m+1}{m}}\left(\underline{U}_e\right)^{\frac{\bar{\Gamma}(m+1)-1}{m}} \tag{63}$$

which is identical to equation (56) except for the substitution of $\bar{\Gamma}$ for Γ. Solutions are therefore given by equations (57a) or (57b) for appropriate initial conditions with Γ replaced by $\bar{\Gamma}$.

The energy equation (47) is solved in the same manner. When Γ is replaced by $\bar{\Gamma}$, equation (47) becomes a linear differential equation of the form

$$\frac{dZ}{d\xi} + Zf_1(\xi) = f_2(\xi) \tag{64}$$

where now

$$f_1(\xi) = \frac{A_m\left(\underline{U}_e\right)^{-\frac{1}{m}}}{\Theta}\left(1 + \frac{\bar{\theta}}{\bar{\lambda}}\right) + \frac{1}{H_e^*}\frac{dH_e^*}{d\xi} - \left(\bar{\Gamma} - 1 - \alpha\frac{H_e^*}{H_e}\frac{\bar{\theta}}{\bar{\lambda}}\right)\frac{1}{\underline{U}_e}\frac{d\underline{U}_e}{d\xi} \tag{65a}$$

$$f_2(\xi) = \frac{\Lambda}{\underline{U}_e}\frac{d\underline{U}_e}{d\xi} - \frac{1}{H_e^*}\frac{dH_e^*}{d\xi} \tag{65b}$$

The general solution is

$$Z = e^{-\int f_1(\xi)d\xi}\left[\int e^{\int f_1(\xi)d\xi} f_2(\xi)d\xi + K\right] \tag{66}$$

As in the special case, equation (66) must be evaluated numerically for arbitrary transition because of the form of the function Θ (eq. (57a)). For the special case of $\Theta_t = \xi_t = 0$, however, a simple analytic solution may again be derived. Thus, when the method used in the case $H_e^* = 0$ is followed here, the result is

$$Z = \frac{\left(\underline{U}_e\right)^{\overline{\Gamma}-1-\alpha\frac{H_e^*}{H_e}\frac{\overline{\theta}}{\overline{\lambda}}}}{H_e^*(F)^{\frac{m}{m+1}\left(1+\frac{\overline{\theta}}{\overline{\lambda}}\right)}} \int_0^{\xi} \frac{H_e^*(F)^{\frac{m}{m+1}\left(1+\frac{\overline{\theta}}{\overline{\lambda}}\right)}}{\left(\underline{U}_e\right)^{\overline{\Gamma}-1-\alpha\frac{H_e^*}{H_e}\frac{\overline{\theta}}{\overline{\lambda}}}} \left(\frac{\Lambda}{\underline{U}_e}\frac{d\underline{U}_e}{d\xi} - \frac{1}{H_e^*}\frac{dH_e^*}{d\xi}\right) d\xi \tag{67}$$

In the interest of simplicity, the case of arbitrary transition (eqs. (57a) and (66)) for the approximate solution will not be considered further. The approximate solution is given by equations (57b) and (67) and is therefore restricted to the initial conditions $\Theta_t = \xi_t = 0$, $Z_t = Z_o$ or fully developed turbulent flow from the leading edge.

Stagnation-region solutions for the approximate case may be obtained from equations (57b) and (67). For a three-dimensional stagnation region,

$$\Theta = A_m \left[\frac{a_o}{\left(\underline{\rho}\,\underline{\mu}\,\underline{r}\right)_o}\right]^{-\frac{1}{m}} \frac{(\xi)^{\frac{m-1}{m}}}{\overline{\Gamma}_o + \frac{2m}{m+1}} \tag{68}$$

$$Z = Z_o = \frac{\Lambda_o}{1 + \alpha\left(\frac{H_e^*}{H_e}\right)_o \frac{\overline{\theta}}{\overline{\lambda}} + \overline{\Gamma}_o \frac{\overline{\theta}}{\overline{\lambda}} + \frac{2m}{m+1}\left(1 + \frac{\overline{\theta}}{\overline{\lambda}}\right)} \tag{69}$$

and for a two-dimensional stagnation region,

$$\Theta = A_m \left[\frac{a_o}{\left(\underline{\rho}\,\underline{\mu}\,\underline{r}\right)_o}\right]^{-\frac{1}{m}} \frac{(\xi)^{\frac{m-1}{m}}}{\overline{\Gamma}_o + \frac{m-1}{m+1}} \tag{70}$$

$$Z = Z_o = \frac{\Lambda_o}{1 + \alpha\left(\frac{H_e^*}{H_e}\right)_o \frac{\overline{\theta}}{\overline{\lambda}} + \overline{\Gamma}_o \frac{\overline{\theta}}{\overline{\lambda}} + \frac{m-1}{m+1}\left(1 + \frac{\overline{\theta}}{\overline{\lambda}}\right)} \tag{71}$$

The three- and two-dimensional stagnation values of Z_o as given by equations (69) and (71), respectively, have also been plotted on figures 2(a) and 2(b), for $\alpha = 1$, $n = 7$, and $m = 4$ and do not differ significantly from the appropriate (negative root) values for the "exact" solution evaluated in the appendix.

For clarification of the two methods discussed herein, a summary is presented in table I.

Reference Conditions

The constant reference conditions ρ_o, μ_o have been used as the pertinent properties for the flow in the transformed (incompressible) plane. This "incompressible" reference is assigned to the stagnation point in the case of a blunt body and local stagnation conditions for bodies with sharp leading edge. This requirement specifies isentropic flow along the body streamline in the inviscid flow for the latter case.

The reference conditions in the boundary layer ρ_r, μ_r are somewhat more arbitrary. The original transformation (ref. 9) for laminar flow used the relation $\rho\mu = 1$, whereas reference 14 used the wall conditions ρ_w, μ_w. The choice of reference conditions in the laminar case influences the form of the transformed equations but not the solutions in the physical plane (except through the viscosity law chosen), since the solutions do not depend upon any assumptions as to the nature of the flow in the transformed plane. Because the turbulent solutions depend upon the assumption that incompressible relations are valid in the transformed plane, the reference conditions need to be carefully specified as follows.

T_w method.- If the laminar shear at the wall was considered and then transformed, this would give

$$\left.\begin{aligned} \tau_w &= \mu_w\left(\frac{\partial u}{\partial y}\right)_w \\ &= \frac{\rho_w\mu_w}{\rho_o\mu_o}\,\frac{h_e}{h_o}\,\mu_o\left(\frac{\partial U}{\partial Y}\right)_w \end{aligned}\right\} \tag{72}$$

If the quantity $\mu_o\left(\frac{\partial U}{\partial Y}\right)_w$ were interpreted as the transformed wall shear $\bar{\tau}_w$, then equation (72) would be

$$\bar{\tau}_w = \frac{\rho_o \mu_o}{\rho_w \mu_w} \frac{h_o}{h_e} \tau_w \tag{73}$$

Comparison of equations (73) and (20) indicates that the reference condition, for this interpretation, must be the wall condition. For the flat plate this comparison gives, from equation (A6),

$$\frac{c_f}{\bar{c}_f} = \left(\frac{\rho_w \mu_w}{\rho_e \mu_e}\right)^{\frac{m}{m+1}} \left(\frac{\mu_e}{\mu_o}\right)^{\frac{n-1}{n+1}} \tag{74}$$

T' method.- In reference 16, an intermediate temperature method for turbulent flow is described. This method has been adapted to the flat-plate inverse power friction law as follows: Assume

$$c_f' \equiv \frac{\tau_w}{\frac{1}{2} \rho' u_e^2} = K_1 \left(\frac{\rho' u_e x}{\mu'}\right)^{-\frac{1}{m+1}}$$

where K_1 is the coefficient of the equivalent incompressible law and ρ' and μ' are evaluated at an intermediate temperature T'. Then

$$c_f = c_f' \frac{\rho'}{\rho_e} = K_1 \left(\frac{\rho_e u_e x}{\mu_e}\right)^{-\frac{1}{m+1}} \left(\frac{\rho'}{\rho_e}\right)^{\frac{m}{m+1}} \left(\frac{\mu'}{\mu_e}\right)^{\frac{1}{m+1}}$$

If for incompressible flow

$$\bar{c}_f = K_1 \left(\frac{\rho u_e x}{\mu}\right)^{-\frac{1}{m+1}}$$

Then at the same Reynolds number

$$\frac{c_f}{\bar{c}_f} = \left(\frac{\rho'}{\rho_e}\right)^{\frac{m}{m+1}} \left(\frac{\mu'}{\mu_e}\right)^{\frac{n-1}{m+1}} \tag{75}$$

The intermediate temperature is given for air by reference 16 as

$$\frac{T'}{T_e} = 1 + 0.035 M_e^2 + 0.45 \left(\frac{T_w}{T_e} - 1\right) \tag{76}$$

The wall reference method (eq. (74)) is compared with the intermediate temperature method (eqs. (75) and (76)) in figure (4) by means of plots of the variation of $c_f/\bar{c}_f$ with Mach number for wall-to-stream-temperature ratios of 0.2, 1, and 5. For this figure it was assumed that the surface was at a temperature of $1{,}500^\circ$ R for all Mach numbers, a fairly realistic condition for a reentry vehicle. Values of γ of 1.4 and m of 4 and the Sutherland viscosity law were used. For this case it is apparent that the two methods are significantly different.

The same two methods are compared for the insulated wall case in figure 5 with a typical wind-tunnel condition imposed, namely, T_o equal to 540° R. A recovery factor equal to $(N_{Pr})^{1/3}$ was used with N_{Pr} equal to 0.72. Also shown on the figure are the experimental data of Coles (ref. 17) and Chapman and Kester (ref. 18) taken from reference 16. There is some tendency for the data to support the T' method over the T_w method. Further support for use of the T' method is found in data recently obtained by Tendeland (ref. 19) for flow with heat transfer.

The assumption is now made that the flat-plate T' method is correct for arbitrary pressure gradient. The reference conditions for the present method are computed by requiring the equivalence of the T' compressibility correction to that of the present report (eq. (A6)). The result of equating equation (A6) with equation (75) is

$$\frac{\rho_r \mu_r}{\rho_o \mu_o} = \frac{\rho'}{\rho_o}\left(\frac{\mu'}{\mu_o}\right)^{1/m} \tag{77}$$

with ρ' and μ' evaluated at T' (eq. (76)). However, for completeness, the T_w method, given by equation (74), obtained from

$$\frac{\rho_r \mu_r}{\rho_o \mu_o} = \frac{\rho_w \mu_w}{\rho_o \mu_o} \tag{78}$$

is evaluated as an alternate.

RESULTS AND DISCUSSION

Method of Calculation

Equations (46) and (47) for the "exact" method and equations (57b) and (67) for the approximate method were solved for various configurations on the IBM 704 card-programed computer at the Langley Aeronautical Laboratory. In order to simplify the programing, the equations were rewritten with the physical dimensionless coordinate $\underline{x}$ as the independent variable as follows:

$$\frac{d\Theta}{d\underline{x}} + \left(\frac{m+1}{m}\right)\left(\frac{\Gamma}{\underline{U}_e}\frac{d\underline{U}_e}{d\underline{x}} + \frac{1}{\underline{r}}\frac{d\underline{r}}{d\underline{x}}\right)\Theta = A_m\left(\frac{m+1}{m}\right)\underline{\rho}_r\underline{\mu}_r\left(\underline{h}_e\right)^{\frac{1}{2}}\left(\underline{U}_e\right)^{-\frac{1}{m}} \tag{79}$$

$$\frac{dZ}{d\underline{x}} + Z\left[\frac{A_m\left(\underline{U}_e\right)^{-\frac{1}{m}}}{\Theta}\left(\underline{\rho}_r\underline{\mu}_r\right)\left(\underline{h}_e\right)^{\frac{1}{2}}\left(1+\frac{\bar{\epsilon}}{\bar{\lambda}}\right) + \frac{1}{H_e^*}\frac{dH_e^*}{d\underline{x}} - \left(\Gamma - 1 - \alpha\frac{H_e^*}{H_e}\frac{\bar{\theta}}{\bar{\lambda}}\right)\frac{1}{\underline{U}_e}\frac{d\underline{U}_e}{d\underline{x}}\right] + \frac{1}{H_e^*}\frac{dH_e^*}{d\underline{x}} - \frac{\Lambda}{\underline{U}_e}\frac{d\underline{U}_e}{d\underline{x}} = 0 \tag{80}$$

for the exact case, and

$$\Theta = A_m\left(\frac{m+1}{m}\right)\left(\underline{U}_e\right)^{-\frac{1}{m}}\frac{F}{\left(\underline{r}\right)^{\frac{m+1}{m}}\left(\underline{l}_e\right)^{\frac{\bar{\Gamma}(m+1)-1}{m}}} \tag{81}$$

$$Z = \frac{\left(\underline{U}_e\right)^{\bar{\Gamma}-1-\alpha\frac{H_e^*}{H_e}\frac{\bar{\theta}}{\bar{\lambda}}}}{H_e^*(F)^{\frac{m}{m+1}\left(1+\frac{\bar{\theta}}{\bar{\lambda}}\right)}}\int_0^{\underline{x}}\frac{H_e^*(F)^{\frac{m}{m+1}\left(1+\frac{\bar{\theta}}{\bar{\lambda}}\right)}}{\left(\underline{U}_e\right)^{\bar{\Gamma}-1-\alpha\frac{H_e^*}{H_e}\frac{\bar{\epsilon}}{\bar{\lambda}}}}\left(\frac{\Lambda}{\underline{U}_e}\frac{d\underline{U}_e}{d\underline{x}} - \frac{1}{H_e^*}\frac{dH_e^*}{d\underline{x}}\right)d\underline{x} \tag{82}$$

for the approximate case where

$$F \equiv \int_0^{\underline{x}}\left(\underline{r}\right)^{\frac{m+1}{m}}\left(\underline{U}_e\right)^{\frac{\bar{\Gamma}(m+1)-1}{m}}\left(\underline{\rho}_r\underline{\mu}_r\right)\left(\underline{h}_e\right)^{1/2}d\underline{x} \tag{83}$$

Because all available data were obtained in the moderate temperature regime, the program was specialized to the case $\alpha = 1$ (constant specific heats) and flow properties outside the boundary layer evaluated in the program from the pressure distribution by simple isentropic-flow relations with constant γ. The viscosity was assumed to be given by the Sutherland law

$$\mu \propto \frac{T^{3/2}}{T + 198.7^{\circ}\ R}$$

The program was arranged for arbitrary selected values of the constants A_m, m, n, $\bar{\delta}_1/\bar{\theta}$, $\bar{\theta}/\bar{\lambda}$, and N_{Pr}. The enthalpy recovery factor η_r was assumed to be equal to $(N_{Pr})^{1/3}$ and the enthalpy difference $H_{aw}{}^*$ was computed from

$$H_{aw}{}^* = H_e\left(\frac{h}{H_e} + \eta_r \frac{u_e^2}{H_e} - \frac{H_w}{H_e}\right)$$

For purposes of comparison, both T' and T_w methods for computing compressibility effects were included in the program.

Unless otherwise specified in the subsequent discussion, the following constants were used:

Blasius law:

$$A_m = 0.013 \qquad m = 4$$

1/7th-power velocity profile:

$$n = 7 \qquad \frac{\bar{\delta}_1}{\bar{\theta}} = \frac{9}{7} \qquad \frac{\bar{\theta}}{\bar{\lambda}} = \frac{5}{4}$$

$$\gamma = 1.4 \qquad N_{Pr} = 0.72$$

Determination of Effect of Initial (Transition) Conditions

In order to determine the effect of various transition conditions upon solutions of the "exact" equations, the discussion which follows assumed instantaneous transition from laminar flow at some location x_t. For this discussion, the reference temperature as evaluated by the T' method (eqs. (76) and (77)) is used.

No exact transition boundary conditions are known. One reasonable conditions is to assume that momentum is conserved; thus $\theta_{laminar}$ equals $\theta_{turbulent}$ at $\underline{x}_t$. An analogous procedure to determine Z_t is to conserve the enthalpy convection thickness φ. The purpose of figures 6 to 12 is to indicate the degree to which the results are affected by various transition boundary conditions.

In figures 6, 7, and 8 are plotted θ/l, Z, and $\frac{q_w}{T_w - T_{aw}}$, respectively, as computed for a hemisphere in a $M = 5$ stream. The test is reported in reference 20 as run 57. Transition was assumed to occur at $\underline{x}_t = 0.4$, 0.6, and 0.8 with $\left(\frac{\theta}{l}\right)_t$ chosen as equal to the appropriate laminar value (computed from the similar solutions of ref. 14 by using a technique similar to that of Stine and Wanlass (ref. 21)). The term Z_t was allowed to vary for each value of $\underline{x}_t$. For each $\underline{x}_t$ the choice of Z_t has little effect on the solutions for Z and $q_w/(T_w - T_{aw})$ except in the immediate vicinity of $\underline{x}_t$. There is no noticeable effect upon θ/l at all.

The choice of $\underline{x}_t$ and $\left(\frac{\theta}{l}\right)_t$ has greater influence upon the results, as may be seen in figures 9 to 11. Since the choice of Z_t was shown to influence only weakly the solutions for given $\underline{x}_t$ and $\left(\frac{\theta}{l}\right)_t$, for these three figures Z_t was set equal to the value of Z at $\underline{x}$ equals $\underline{x}_t$ obtained from the solution for the stagnation initial conditions $\left(\underline{x}_t = \left(\frac{\theta}{l}\right)_t = 0, \quad Z_t = Z_o\right)$ which are also shown in figures 6 to 12. For given $\underline{x}_t$, the choice of $\left(\frac{\theta}{l}\right)_t$ strongly affects the solutions locally, the effect diminishing downstream. In addition, increasing $\underline{x}_t$ increases the effect of varying $\left(\frac{\theta}{l}\right)_t$; that is, the effect is felt further downstream, as expected.

The data obtained in reference 20 appear to favor the solutions with large $\left(\frac{\theta}{l}\right)_t$ with Z_t fixed near $\underline{x} \cong 0.8$ and to favor the solutions with $\left(\frac{\theta}{l}\right)_t = \left(\frac{\theta}{l}\right)_{laminar}$ at $\underline{x}_t = 0.6$ and 0.8 in the region $\underline{x} > 1.0$.

The results of similar calculations for heat-transfer coefficient on a flat-faced body are shown in figure 12. The conditions are those of run 61 of reference 20. Transition was assumed to occur at $\underline{x}_t = 0.2$, 0.4, and 0.6 for various values of $\left(\frac{\theta}{l}\right)_t$. Because of the previously shown negligible effect of Z_t, the values of Z_t were chosen in the same manner as for the hemisphere (figs. 9 to 11). Figure 12 shows the same behavior for the flat-faced model as found for the hemisphere, that is, the effect of $\left(\frac{\theta}{l}\right)_t$ decreases with increasing $\underline{x}$ and, when $\underline{x}_t = 0.2$ or 0.4, does not appear to be important a moderate distance from the assumed transition point. The experimental data for this flat-faced body are plotted in figure 12 and appear to favor transition at $\underline{x}_t$ equals 0.4 with $\left(\frac{\theta}{l}\right)_t$ equal to 0.00072 or 0.00108.

Some investigators have advocated starting the turbulent calculation from the stagnation point with finite initial momentum thickness. (See, for example, ref. 5.) They reason that a nonzero boundary-layer thickness must exist at a stagnation point, such as the laminar value which is easily calculated. Solutions for the present method were obtained for a wide range of $\left(\frac{\theta}{l}\right)_t$ for $\underline{x}_t$ equal to zero for both spherical and flat-faced bodies. These results showed that the perturbations in $\left(\frac{\theta}{l}\right)$, Z, and $q_w/\left(T_w - T_{aw}\right)$ caused by the nonzero $\left(\frac{\theta}{l}\right)_t$ die out extremely rapidly and are indistinguishable from those for $\left(\frac{\theta}{l}\right)_t = 0$, $\underline{x}_t = 0$, downstream of $\underline{x} = 0.25$. These results have not been shown in figures 9 to 12. Since the flow in the region close to the stagnation point is expected to be laminar, it must be concluded that for all practical purposes the assumption of finite $\left(\frac{\theta}{l}\right)_t$ at the stagnation point for the present method is practically equivalent to the assumption of zero $\left(\frac{\theta}{l}\right)_t$.

Figures 6 to 12 show that the "exact" solution started at the stagnation point fairly well represents the solutions begun at an assumed transition point, particularly for early transition. Therefore, this solution is useful when the location of transition is unknown. However, use of stagnation-point initial conditions does not imply that turbulent flow exists over the whole surface but merely assumes that the turbulent flow downstream of transition is approximately equivalent to a hypothetical turbulent flow which originates at the stagnation point.

Comparison of Present Method With Experiment

Results of application of the present method are shown in figures 13 to 19 corresponding to experimental data presented in references 20, 22, and 23. Both exact and approximate solutions were evaluated with the calculation restricted to the isothermal-wall case. This condition was very nearly met in all the experiments discussed. The values of H_w/H_e chosen were approximate means of the local values and are indicated in table II, a summary of the experimental data used in the figures. In all cases the experimental pressure distributions presented in the references were used.

The exact method was evaluated for stagnation initial conditions $\left(\underline{x}_t = \Theta_t = 0, \quad Z_t = Z_o\right)$ and, for one transition case in which $\underline{x}_t$ was chosen from the experimental data, Θ_t was assumed equal to the laminar value and Z_t was arbitrarily set equal to its value at $\underline{x} = \underline{x}_t$ as given by the solution for stagnation initial conditions. Use of stagnation initial conditions was implicit in the approximate solution.

Plotted in these figures is the variation of the heat-transfer coefficient $\frac{q_w}{T_w - T_{aw}}$ with the dimensionless surface distance $\underline{x} \equiv \frac{x}{l}$. The reference length is the body radius for the hemisphere and flat-faced body of reference 20 (figs. 13 and 14) and the hemispheres of reference 22 (figs. 15 and 16), and the nose radius for the sphere cones of reference 23 (figs. 17, 18, and 19). In each case the (a) parts of the figures correspond to the T' method, and the (b) parts of the figures, to the T_w method.

Examination of the figures reveals the following:

(1) In general, the results using the T' method for $c_f/\overline{c}_f$ are slightly higher (generally less than 5 percent higher in the peak heating region) than those with $c_f/\overline{c}_f$ given by the T_w method. The data show a slight preference for the T' method.

(2) The approximate solution gives results within 5 percent of those of the exact solution using stagnation-point initial conditions. Neither of these methods predicts completely the experimental data, although most trends not too close to the transition region are satisfactorily predicted.

(3) The exact solution with transition initial conditions predicts the measured peak heat-transfer data within approximately 10 percent in those cases where transition appears to have begun upstream of the

theoretical peak (figs. 15, 18, and 19). In figures 15 and 18, the location of the theoretical peak is slightly upstream of the experimental location. When transition appears to have begun close to the predicted peak heating region (figs. 13, 16, and 17), agreement at the peak may be either good (within 15 percent, fig. 16) or poor (figs. 13 and 17). In these three cases the peak heating data are thought to be transitional.

(4) Downstream of the peak heating regions agreement is generally within 10 percent except for the extreme downstream locations where heating rates are low and percent differences between theory and experiment tend to increase (figs. 13 and 15 to 19). An exception is the flat-faced body where the predicted heating rates are 20 to 25 percent greater than the experimental rates over the entire face.

(5) Using a transition initial condition in preference to stagnation initial conditions generally improves or leaves unchanged agreement between "exact" theory and experiment except in two of the cases where the peak heating data are thought to be transitional. (See figs. 13 and 17.)

In regard to these comparisons, caution must be exercised in quantitatively comparing data and theory as a 10 to 20 percent uncertainty is common in heat-transfer measurements. The question of choosing transition conditions for the present method leads to further uncertainty. Although the technique of requiring conservation of momentum thickness may appear to be logical for an instability-induced transition, a roughness-induced transition might suggest a discontinuous momentum thickness. Figures 11 and 12 demonstrate how transition with θ_t larger than $\theta_{laminar}$ can lead to better agreement between theory and experiment for the same data as in figures 13 and 14, respectively. In both of these cases, transition may be roughness induced. (See ref. 20.)

Comparison With Other Methods

Comparison with Dennison's method.- The method of Dennison has been evaluated for the seven experimental configurations previously discussed. A simplified form which Dennison states is valid only on the forebodies of blunted cones and cylinders and invalid far downstream has been used along with a Prandtl number correction in the modified Reynolds analogy suggested by Dennison and used also in the present analysis. The results are shown in the (a) parts of figures 13 to 19 in each case, although Dennison's method is not dependent upon a reference-temperature compressibility correction. The comparisons made in the following paragraph refer only to the present T' method and Dennison's method.

The method of Dennison appears to predict heating rates about as well, in general, as does the present method with stagnation initial conditions. The present method with transition predicts the peak heating rates much more accurately than does Dennison's method for the configurations of figures 15, 16, 18, and 19. For the hemisphere at $M = 5$ (fig. 13) and the sphere cone (fig. 17), the Dennison predictions are closer to the peak heating rates than the present solutions, which overpredict the experimental peak heating rates However, these measurements appear to be in a transition region. Heating rates on the flat-faced body at $M = 5$ (fig. 14) are predicted by Dennison's method with excellent accuracy.

Comparison with incompressible flat-plate formula.- In order to provide a familiar reference curve in figures 13 to 19, the heat-transfer rate was computed by using the Blasius incompressible flat-plate law and Reynolds analogy with the assumption of no effect of compressibility upon skin friction. The equations are

$$\frac{c_f}{2} = 0.0296\left(N_{Re}\right)^{-\frac{1}{5}}$$

$$\frac{q_w}{T_w - T_{aw}} = c_p \rho_e u_e \left(N_{Pr}\right)^{-\frac{2}{3}} \frac{c_f}{2}$$

The results of using these simple relations are also plotted on the (a) parts of figures 13 to 19. This method, however, is independent of compressibility.

Although these results agree with the more complete results of the present analyses as well as with Dennison's method and data in some regions, differences are rather large over most of the surfaces. The occasional agreement is the result of compensating effects. The present method includes the effect of the favorable pressure gradient upon momentum thickness in the momentum equation. This tends to increase the skin-friction coefficient over the comparable flat-plate value. On the other hand, the effect of pressure gradient upon the Reynolds analogy factor is such that the ratio of heat-transfer rate to skin-friction coefficient is reduced below the comparable flat-plate value. In some regions these effects approximately cancel and agreement between the pressure gradient and flat-plate solutions results, particularly for the flat-nosed body. (See fig. 14.) In other regions one effect predominates and the solutions do not agree at all. The compressibility correction factor included in the present method further alters the comparison. Because of this fortuitous part-time agreement, the incompressible flat-plate method is not suitable for blunt-nosed bodies. In the figures discussed here, this method yields heat-transfer rates generally higher than the data or the results of the pressure-gradient methods.

The method of Bloom and Martellucci.- Bloom and Martellucci (ref. 6) use the integrated momentum and energy equations to derive a modified Reynolds analogy relation analogous to that of equation (4) of the present report. This relation is used in conjunction with an inverse power friction law, power velocity profile, reference-temperature compressibility correction, and a relation between total enthalpy and velocity independent of pressure gradient in order to obtain the heat-transfer rate. The results of these calculations are not included in the present report but were shown in references 4 and 6 to underestimate seriously the turbulent heating rates on a blunt body. This behavior must be attributed to the form of the enthalpy-velocity relation used. By not including the effects of pressure gradient in the total enthalpy profile, a modified Reynolds analogy factor q_w/τ_w which depends directly on velocity gradient is obtained, which is analogous to equation (4) herein. This relation shows that positive velocity gradients tend to reduce drastically the Reynolds analogy factor and yield low heating rates. When the pressure gradient is included in the enthalpy profile, however, as in the present analysis, the modified Reynolds analogy factor depends instead upon an integral of the velocity gradient (for example, eq. (67) for Z), and thus the effect of pressure gradient is reduced. This result is apparent in the generally satisfactory agreement between measured heating rates and those predicted by the present method as shown in figures 13 to 19.

Discussion

Choice of initial conditions for the exact solution and validity of the approximate solution.- In a previous section it was shown that the choice of initial conditions at the transition point did not seriously affect the predicted heat-transfer rates a moderate distance downstream of the assumed transition point. With no real knowledge of what transition conditions to use, figures 13 to 19 show that use of stagnation initial conditions can lead to reasonably accurate predictions of the turbulent heating rates a moderate distance downstream of the transition point or region. It follows, then, that the approximate method presented herein may also be very useful, in spite of the fact that it requires stagnation initial conditions. Results of using this method also compare very favorably with the experimental data.

If it is desired to utilize high-speed computing equipment in the calculation of turbulent heat transfer by the present method, the exact solution should be employed as it offers the generality of arbitrary initial (transition) conditions as well as exactness (within the framework of all the other assumptions). Where no such equipment is available, the approximate method offers a convenient alternative restricted to stagnation initial conditions. One might improve the accuracy of

the approximate method by a more judicious choice of a mean value of Z used in evaluating $\bar{\Gamma}$ (eq. (62)) but the need for doing so is not apparent in the present results. Caution must be used in applying this approximation, however, as it was derived by neglecting $dZ/d\xi$ with respect to $dU_e/d\xi$, a questionable assumption in the essentially zero pressure-gradient downstream regions of blunted cones or cylinders. In a subsequent section, this error is shown to be small for one case - a spherically blunted cylinder in shock-tube flow.

An alternate friction law.- In order to determine the effect of changing the friction law, the heat-transfer coefficients for the hemisphere and flat-faced bodies at Mach number of 5 (ref. 20) were computed for the friction law

$$\frac{\bar{c}_f}{2} = 0.0065\left(\frac{\rho_o U_e \bar{\theta}}{\mu_o}\right)^{-\frac{1}{6}}$$

given in reference 3 and attributed to Falkner (ref. 24). Results of these calculations are shown in figures 20 and 21 for hemispherical and flat-face bodies, respectively. Also shown are the results obtained by using $A_m = 0.013$ and $m = 4$ (modified Blasius law) as in the previous discussion, and the experimental results. Theoretical results are shown only for the special case where the flow is considered to be turbulent from the stagnation point $\left(\underline{x}_t = \Theta_t = 0, \quad Z_t = Z_o\right)$ for the exact solution (T' method).

For a flat plate in incompressible flow, the modified Blasius law is considered to be a good approximation to the Prandtl-Schlichting logarithmic law for Reynolds numbers based on surface distances of from 10^5 to 10^7, and the Falkner law may be used to approximate the logarithmic law for Reynolds numbers of from 10^6 to 10^{10}. Approximate Reynolds number limitations such as these may be considered to be appropriate for the calculation of heat transfer by the present method. For the experiments considered herein, Reynolds numbers based upon local external fluid properties and surface distance from the stagnation point never exceeded 2.5×10^6; thus, the Blasius law should be appropriate. Figure 20 for the hemisphere shows little difference in the two results, although the Blasius result is slightly closer to the data downstream of the transition region. Figure 21 for the flat-faced body shows that the Falkner result agrees with the data very closely, whereas the Blasius result averages about 20 percent high. This behavior remains unexplained.

If it were desired to compute heating rates by the present method to a body for which the local Reynolds number based upon surface distance covered both of these ranges, the calculation could begin with the

Blasius law carried up to an appropriate location and then continue with the Falkner law for the remainder of the surface, with the requirement that θ and Z were continuous at the "switchover point." The heat-transfer rate would be discontinuous at this point but could easily be faired to obtain a turbulent heating rate continuous in x.

Bloom and Martellucci (ref. 6) used an inverse power friction law with A_m equal to 0.006361 and m equal to 5.92, a law very similar to the Falkner relation. They also claimed to have computed one case by using a Blasius law $(A_m = 0.0128, \quad m = 4)$ and, when the results were compared, they found a difference of nearly a factor of 2. They appear to have used a value of A_m equal to 0.0225 in the actual calculations, however, and its use would account for the discrepancy.

Validity of the approximate method in downstream regions.- The accuracy of the approximate solution in the downstream region of a spherically blunted cylinder was tested for a hypothetical shock-tube situation. The model was assumed to be one-half inch in diameter, and the traveling shock was assumed to move at a Mach number of 6.5 relative to the fixed wall and based upon the speed of sound of the undisturbed air, which was assumed at room temperature (540° F) and a pressure of 40 centimeters mercury absolute. Local flow conditions around the model were found by assuming a modified Newtonian pressure distribution; stagnation conditions were computed from the charts of reference 25. For convenience in computing the heat transfer, the flow external to the boundary layer was assumed to be isentropic with γ equal to 1.2. The wall temperature was assumed to be equal to room temperature, a valid assumption for the short-duration tests inherent in shock-tube use, and the computed stagnation temperature was 6,318° R.

Figure 22 shows a plot of the variation of the ratio of local heat-transfer rate to stagnation heat-transfer rate (computed by the method of ref. 13) for exact and approximate solutions with $\underline{x} \equiv x/l$, where l is the body radius. Only the T' method is shown, and only stagnation initial conditions are chosen for the exact solution. Equation (76) for T' is assumed to be valid independent of γ. The region $\underline{x} < 1.57$ corresponds to the hemispherical nose, and the region $\underline{x} > 1.57$ represents the downstream cylinder. Figure 22 shows that the approximate solution differs from the exact by less than 5 percent over the entire surface considered, $\underline{x} \leq 3.0$. This result is surprising in the region where $\underline{x} > 1.57$, since in this region the Newtonian velocity gradient is zero whereas the gradient of Z is still finite. In obtaining the approximate solution, $dZ/d\xi$ was neglected as small compared with $d\underline{U}_e/d\xi$, an assumption which is not true for $\underline{x} > 1.57$. This relative insensitivity to the neglect of the $dZ/d\xi$ terms in the downstream regions somewhat widens the applicability of the approximate solution presented herein.

CONCLUDING REMARKS

A method for computing the turbulent heat transfer to bodies in high-speed two-dimensional and axisymmetric flow fields was derived from the integrated equations of the boundary layer. The derivation utilized a Stewartson-type transformation of the equations, the assumption of a quadratic dependence of total enthalpy upon velocity across the boundary layer (in which the coefficients of the velocity terms are functions of pressure gradient), and a compressibility correction for skin-friction coefficient based upon flat-plate experimental data. The method was applied specifically for inverse-power-law velocity profiles and friction coefficients. Exact and approximate solutions were derived for these differential equations wherein the exact solution was valid for any initial conditions, and the approximate solution required assumption of a fully developed turbulent flow from stagnation point or leading edge with appropriate initial conditions. A primary result of the derivation was the existence, within the present assumptions, of a modified Reynolds analogy between heat transfer and skin friction for turbulent flow, a relation which depends upon streamwise pressure gradient.

Examination of the exact solution for various initial conditions (representing a variety of transition values) for flow about a hemisphere and a flat-faced body indicated that choice of the initial condition would influence the result close to the transition point but that this influence would decay in the downstream regions. It was shown that hypothetical initial conditions at a stagnation point or leading edge led to a solution which would satisfactorily approximate those solutions with arbitrary initial conditions downstream of their respective initial streamwise location.

Comparison of the present results with available experimental heat-transfer data on seven axisymmetric blunt bodies showed general agreement between experiment and theory, in most cases within the experimental accuracy. Use of a transition initial condition in preference to a stagnation initial condition tended to improve agreement between experiment and exact theory except for cases where transition appeared to begin in the region of peak predicted heat transfer. Results using the approximate solution never deviated from those of the exact solution with stagnation initial conditions by more than 5 percent.

The present method appears to be capable of predicting turbulent heat transfer with sufficient accuracy for design purposes, except perhaps close to transition. Although the exact solution offers the generality of arbitrary transition initial conditions, the computation is sufficiently involved to make desirable the employment of high-speed automatic computing equipment. In the absence of specific knowledge of

the transition phenomenon, the assumption of fully developed turbulent flow from the stagnation point or leading edge still leads to highly useful predictions in the region where the flow is actually turbulent. With this assumption, the approximate solution has value in that it lends itself to hand calculation with little loss of accuracy.

The present method is restricted to flow without dissociation. Variable specific heats may be included in an approximate manner; however, no experimental data including this effect were available for comparison.

Langley Research Center,
National Aeronautics and Space Administration,
Langley Field, Va., September 30, 1958.

APPENDIX

SPECIAL CASES

Under certain conditions, equations (46) and (47) may be solved analytically. The case with $H_e^* = 0$ is treated in the text. Some additional examples are shown in the following sections.

Flat Plate or Cylinder With Sharp Leading Edge, Constant Specific Heat

For the flat plate or cylinder with sharp leading edge and constant specific heat, the equations are simplified by the restriction $\frac{du_e}{dx} = \frac{dr}{dx} = 0$, $\alpha = 1$. Equation (46) is integrated immediately and the following equation results:

$$\Theta = \Theta_t + A_m\left(\frac{m+1}{m}\right)\left(\underline{U}_e\right)^{-\frac{1}{m}}\left(\xi - \xi_t\right) \tag{A1a}$$

If the flow is assumed to be turbulent from the leading edge, that is, $\Theta_t = \xi_t = 0$, then

$$\Theta = A_m\left(\frac{m+1}{m}\right)\left(\underline{U}_e\right)^{-\frac{1}{m}}\xi \tag{A1b}$$

The skin friction for an all-turbulent flow is found from equations (41) and (A1b) to be

$$\frac{\overline{c}_f}{2} = \left(A_m\right)^{\frac{m}{m+1}}\left(\frac{m+1}{m}\right)^{-\frac{1}{m+1}}\left(\frac{\rho_c U_e X}{\mu_o}\right)^{-\frac{1}{m+1}} \tag{A2}$$

One example of a friction law is the Blasius pipe-resistance formula as modified in reference 3 for which $A_m = 0.013$ and $m = 4$ and for which equation (A2) becomes

$$\frac{\bar{c}_f}{2} = 0.0296\left(\frac{\rho_o U_e X}{\mu_o}\right)^{-\frac{1}{5}} \tag{A3}$$

The modified Reynolds analogy equation for this case becomes

$$\frac{dZ}{d\xi} + Z\left[\frac{A_m\left(\frac{U_e}{}\right)^{-\frac{1}{m}}}{\Theta}\left(1 + \frac{\bar{\theta}}{\bar{\lambda}}\right) + \frac{1}{H_e^*}\frac{dH_e^*}{d\xi}\right] + \frac{1}{H_e^*}\frac{dH_e^*}{d\xi} = 0 \tag{A4}$$

which is an ordinary linear differential equation with Θ given by equation (Alb). This is of the form

$$\frac{dZ}{d\xi} + f_1(\xi)Z = f_2(\xi)$$

for which the general solution is

$$Z = e^{-\int f_1(\xi)d\xi}\left[\int e^{\int f_1(\xi)d\xi} f_2(\xi)d\xi + K\right]$$

The constant K may be evaluated by consideration of the boundary conditions. When the simple case of constant wall enthalpy is considered,

$$\frac{dH_e^*}{d\xi} \equiv \frac{d\left(H_e - H_w\right)}{d\xi} = 0$$

and a particular solution of (A4) is $Z = 0$. This is the solution of interest, the flat-plate Reynolds analogy.

The relation between compressible and incompressible skin-friction coefficients is computed from the definition of X and $\bar{c}_f$ in conjunction with equation (A2). It is assumed that reference conditions ρ_r and μ_r will, in general, be functions of the local flow outside the boundary layer. For this flat-plate case, then, ρ_r and μ_r are constant. If equations (5a) and (18) are substituted into equation (A2) there results

$$\frac{c_f}{2} = \left(A_m\right)^{\frac{m}{m+1}}\left(\frac{m+1}{m}\right)^{-\frac{1}{m+1}}\left(\frac{\rho_e u_e x}{\mu_e}\right)^{-\frac{1}{m+1}}\left(\frac{\rho_r \mu_r}{\rho_e \mu_o}\right)^{\frac{m}{m+1}}\left(\frac{\mu_e}{\mu_o}\right)^{-\frac{1}{m+1}} \tag{A5}$$

The ratio of the skin frictions is, from equations (A2) and (A5),

$$\frac{c_f}{\bar{c}_f} = \left(\frac{\rho_r \mu_r}{\rho_e \mu_o}\right)^{\frac{m}{m+1}}\left(\frac{\mu_e}{\mu_o}\right)^{-\frac{1}{m+1}} \tag{A6}$$

at the same Reynolds number.

Cone in Supersonic Flow With Attached Shock, Constant Specific Heats

For the cone in supersonic flow with attached shock and constant specific heats, no pressure gradient exists for zero angle of attack; thus, $\frac{du_e}{dx} = \frac{dU_e}{d\xi} = 0$. In this case, however, $r \propto x$ and $\frac{dr}{dx} = \text{Constant}$. The momentum equation (46) becomes

$$\frac{d\left[\Theta\left(\underline{r}\right)^{\frac{m+1}{m}}\right]}{d\xi} = A_m \frac{m+1}{m}\left(\underline{U}_e\right)^{-\frac{1}{m}}\left(\underline{r}\right)^{\frac{m+1}{m}}$$

for which a solution, specialized immediately to $\Theta_t = \xi_t = 0$, is

$$\Theta = A_m\left(\frac{m+1}{m}\right)\left(\underline{U}_e\right)^{-\frac{1}{m}} \frac{1}{\left(\underline{r}\right)^{\frac{m+1}{m}}} \int_0^{\xi} \left(\underline{r}\right)^{\frac{m+1}{m}} d\xi \tag{A7}$$

Since $r \propto x$, then $\underline{r} \propto \xi$ because ρ_r and μ_r are again constant. Equation (A7) becomes

$$\Theta = A_m\left(\frac{m+1}{2m+1}\right)\left(\underline{U}_e\right)^{-\frac{1}{m}} \xi \tag{A8}$$

Combination of equations (41) and (A8) yields

$$\frac{\overline{c}_f}{2} = \left(A_m\right)^{\frac{m}{m+1}}\left(\frac{m+1}{2m+1}\right)^{-\frac{1}{m+1}}\left(\frac{\rho_o U_e X}{\mu_o}\right)^{-\frac{1}{m+1}} \tag{A9}$$

Just as in the case of the flat plate, the solution $Z = 0$ for constant wall enthalpy satisfies the differential equation for Z. Furthermore, the same compressibility correction for skin friction holds (eq. (A6)). Finally, it is apparent when comparing the two cases that

$$\frac{\left(\overline{c}_f\right)_{cone}}{\left(\overline{c}_f\right)_{plate}} = \frac{\left(c_f\right)_{cone}}{\left(c_f\right)_{plate}} = \left(\frac{2m+1}{m}\right)^{\frac{1}{m+1}}$$

at the same Reynolds number and for the same wall and stream conditions. In other words, for the same friction coefficient on cone and plate,

$$\left(N_{Re}\right)_{cone} = \frac{2m+1}{m}\left(N_{Re}\right)_{plate}$$

when wall and stream conditions are the same on cone and plate. For the special case $m = 4$, this relation is

$$\left(N_{Re}\right)_{cone} = \frac{9}{4}\left(N_{Re}\right)_{plate}$$

a result which compares favorably with that of Van Driest (ref. 2) who obtained

$$\left(N_{Re}\right)_{cone} = 2\left(N_{Re}\right)_{plate}$$

Stagnation Region on Two- and Three-Dimensional Bodies

Although turbulent flow at a stagnation point has little physical significance, use of stagnation-point boundary conditions $\left(\underline{x}_t = 0\right)$ in the "exact" differential equations (46) and (47), as well as in the

approximate solution, necessitates a stagnation region solution. Such a solution is easily obtained for the exact case from equations (46) and (47) by requiring that $\underline{u}_e = a_o\underline{x}$, $\underline{r} = \underline{x}$ for axisymmetric flow, and $\underline{u}_e = a_o\underline{x}$ for two-dimensional flow, where a_o is the dimensionless stagnation-point velocity gradient. By this procedure, for a three-dimensional stagnation region,

$$\Theta = A_m\left[\frac{a_o}{\left(\underline{\rho}_r\underline{\mu}_r\right)_o}\right]^{-\frac{1}{m}} \frac{1}{\Gamma_o + \frac{2m}{m+1}}(\xi)^{\frac{m-1}{m}} \tag{A10}$$

$$Z = Z_o = \frac{-d_1 \pm \sqrt{d_1^2 - 4\Lambda_o c\left(\frac{H_e^*}{H_e}\right)_o\left(\frac{\bar{\theta}}{\bar{\lambda}}\right)^2}}{2\alpha\left(\frac{H_e^*}{H_e}\right)_o\left(\frac{\bar{\theta}}{\bar{\lambda}}\right)^2} \tag{A11}$$

and for a two-dimensional stagnation region

$$\Theta = A_m\left[\frac{a_o}{\left(\underline{\rho}_r\underline{\mu}_r\right)_o}\right]^{-\frac{1}{m}} \frac{1}{\Gamma_o + \frac{m-1}{m+1}}(\xi)^{\frac{m-1}{m}} \tag{A12}$$

$$Z = Z_o = \frac{-d_2 \pm \sqrt{d_2^2 - 4\Lambda_o\alpha\left(\frac{H_e^*}{H_e}\right)_o\left(\frac{\bar{\theta}}{\bar{\lambda}}\right)^2}}{2\alpha\left(\frac{H_e^*}{H_e}\right)_o\left(\frac{\bar{\theta}}{\bar{\lambda}}\right)^2} \tag{A13}$$

where

$$-d_1 \equiv 1 + \left(\frac{\bar{\theta}}{\bar{\lambda}}\right)\left[2 + \left(\frac{\bar{\delta}_1}{\bar{\theta}}\right)\left(\frac{H_w}{H_e}\right)_o\right] + \alpha\left(\frac{H_e^*}{H_e}\right)_o\left(\frac{\bar{\theta}}{\bar{\lambda}}\right) + \frac{2m}{m+1}\left(1 + \frac{\bar{\theta}}{\bar{\lambda}}\right) -$$

$$(\alpha - 1)\left(\frac{H_e^*}{H_e}\right)_o\left(\frac{\bar{\delta}_1}{\bar{\theta}}\right)\left(\frac{\bar{\theta}}{\bar{\lambda}}\right) \tag{A14}$$

$$-d_2 = -d_1 - \left(1 + \frac{\overline{\theta}}{\overline{\lambda}}\right) \tag{A15}$$

Two roots appear in each equation for Z_o. The negative root must be chosen as that which gives physically reasonable values of Z_o, that is, between zero and 0.8. (See approximate solution.) This is seen from figure 2, where Z_o for the special case $\alpha = 1$, $n = 7$, $m = 4$ has been plotted against stagnation-point wall cooling ratio $\left(\frac{H_w}{H_e}\right)_o$ for two- and three-dimensional stagnation points (eqs. (A11) and (A13)). It is seen that the negative root is appropriate.

Equations (A11) and (A13) also show that Z is not a function of ξ in the stagnation region, and hence $\left(\frac{dZ}{d\xi}\right)_o = 0$.

REFERENCES

1. Van Driest, E. R.: Turbulent Boundary Layer in Compressible Fluids. Jour. Aero. Sci., vol. 18, no. 3, Mar. 1951, pp. 145-160, 216.

2. Van Driest, E. R.: Turbulent Boundary Layer on a Cone in a Supersonic Flow at Zero Angle of Attack. Jour. Aero. Sci., vol. 19, no. 1, Jan. 1952, pp. 55-57, 72.

3. Schlichting, Hermann (J. Kestin, trans.): Boundary Layer Theory. McGraw-Hill Book Co., Inc., 1955.

4. Libby, Paul A., and Cresci, Robert J.: Evaluation of Several Hypersonic Turbulent Heat Transfer Analyses by Comparison With Experimental Data. WADC Tech. Note 57-72, ASTIA Doc. No. AD 118093, U. S. Air Force, July 1957.

5. Rose, Peter H., Probstein, Ronald F., and Adams, Mac C.: Turbulent Heat Transfer Through a Highly Cooled Partially Dissociated Boundary Layer. Res. Rep. 14, AVCO Res. Lab., Jan. 1958.

6. Bloom, M. H., and Martellucci, A.: A Method for Calculating Turbulent Boundary Layer Properties in High Speed Flow. Tech. Rep. No. 27A, Gruen Appl. Sci. Labs., Inc., Mar. 1957.

7. Cohen, Nathaniel B.: Relations Between Heat, Mass, and Momentum Transfer in Laminar and Turbulent Boundary Layers. RAD-2-TR-57-33, AVCO Res. and Advanced Dev. Div., Sept. 24, 1957. (Supersedes RAD-2-TM-57-58.)

8. Reshotko, Eli, and Tucker, Maurice: Approximate Calculation of the Compressible Turbulent Boundary Layer With Heat Transfer and Arbitrary Pressure Gradient. NACA TN 4154, 1957.

9. Stewartson, K.: Correlated Incompressible and Compressible Boundary Layers. Proc. Roy. Soc. (London), ser. A, vol. 200, No. A1060, June 30, 1949, pp. 84-100.

10. Reshotko, Eli: Simplified Method for Estimating Compressible Laminar Heat Transfer With Pressure Gradient. NACA TN 3888, 1956.

11. Rott, Nicholas: On the Transfer of Heat and Mass in the Turbulent Boundary Layer. Rep. No. GM-TR-211, The Ramo-Wooldridge Corp., Guided Missile Res. Div., July 11, 1957.

12. Mager, Artur: Transformation of the Compressible Turbulent Boundary Layer. Jour. Aero. Sci., vol. 25, no. 5, May 1958, pp. 305-311.

13. Fay, J. A., and Riddell, F. R.: Theory of Stagnation Point Heat Transfer in Dissociated Air. Res. Rep. 1, AVCO Res. Lab., June 1956 (rev. Apr. 1957). (Formerly AVCO Res. Note 18.)

14. Cohen, Clarence B., and Reshotko, Eli: Similar Solutions for the Compressible Laminar Boundary Layer With Heat Transfer and Pressure Gradient. NACA Rep. 1293, 1956. (Supersedes NACA TN 3325.)

15. Ludwieg, H., and Tillman, W.: Investigations of the Wall-Shearing Stress in Turbulent Boundary Layers. NACA TM 1285, 1950.

16. Sommer, Simon C., and Short, Barbara J.: Free-Flight Measurements of Turbulent Boundary-Layer Skin Friction in the Presence of Severe Aerodynamic Heating at Mach Numbers From 2.8 to 7.0. NACA TN 3391, 1955.

17. Coles, D.: Measurements in the Boundary Layer on a Smooth Flat Plate in Supersonic Flow. Ph.D. Thesis, Calif. Inst. Tech., 1953.

18. Chapman, Dean R., and Kester, Robert H.: Turbulent Boundary-Layer and Skin-Friction Measurements in Axial Flow Along Cylinders at Mach Numbers Between 0.5 and 3.6. NACA TN 3097, 1954.

19. Tendeland, Thorval: Effects of Mach Number and Wall-Temperature Ratio on Turbulent Heat Transfer at Mach Numbers From 3 to 5. NACA TN 4236, 1958.

20. Cooper, Morton, and Mayo, Edward E.: Measurements of Local Heat Transfer and Pressure on Six 2-Inch-Diameter Blunt Bodies at a Mach Number of 4.95 and Reynolds Numbers Per Foot up to 81×10^6. NASA MEMO 1-3-59L, 1959.

21. Stine, Howard A., and Wanlass, Kent: Theoretical and Experimental Investigation of Aerodynamic-Heating and Isothermal Heat-Transfer Parameters on a Hemispherical Nose With Laminar Boundary Layer at Supersonic Mach Numbers. NACA TN 3344, 1954.

22. Beckwith, Ivan E., and Gallagher, James J.: Heat Transfer and Recovery Temperatures on a Sphere With Laminar, Transitional, and Turbulent Boundary Layers at Mach Numbers of 2.00 and 4.15. NACA TN 4125, 1957.

23. Ferri, Antonio, Cresci, Robert J., and Libby, Paul A.: Preliminary Hypersonic Laminar and Turbulent Heat Transfer Data Obtained by a New Technique. WADC Tech. Note 56-378, ASTIA Doc. No. AD97237, U. S. Air Force, Dec. 1956.

24. Falkner, V. M.: A New Law for Calculating Drag. The Resistance of a Smooth Flat Plate With Turbulent Boundary Layer. Aircraft Engineering, vol. XV, no. 169, Mar. 1943, pp. 65-69.

25. Feldman, Saul: Hypersonic Gas Dynamic Charts for Equilibrium Air. AVCO Res. Lab., Jan. 1957.

TABLE I.- SUMMARY OF EQUATIONS FOR AND RESTRICTIONS UPON EXACT AND APPROXIMATE SOLUTIONS

Type of solution	Governing equations for Θ and Z	Equation for Γ	Transition boundary conditions
Exact	Eqs. (46) and (47) or eqs. (79) and (80)	Eq. (37a)	Arbitrary
Approximate	Eqs. (57b) and (67) or eqs. (81) and (82)	Eq. (62)	$\underline{x}_t = \Theta_t = 0$, (eqs. (68) or (70)) $Z_t = Z_o$ (eqs. (69) or (71))

TABLE II.- SUMMARY OF EXPERIMENTAL DATA USED TO COMPARE WITH PREDICTED HEATING RATES

Figure	Reference	Remarks
13	20	Run 57; $\frac{H_w}{H_e}$ = 0.663; hemisphere; l = Radius
14	20	Run 61; $\frac{H_w}{H_e}$ = 0.660; flat-faced cylinder; l = Radius of cylinder
15	22	$\frac{H_w}{H_e}$ = 0.49; $F_D = 19.26 \times 10^6$ (notation of ref. 22); hemisphere; l = Radius
16	22	$\frac{H_w}{H_e}$ = 0.77; $F_D = 10.85 \times 10^6$ (notation of ref. 22); hemisphere; l = Radius
17	23	Run 3-12; $\frac{H_w}{H_e}$ = 0.55; sphere-cone; l = Nose radius
18	23	Run 5-8; $\frac{H_w}{H_e}$ = 0.60; sphere-cone; l = Nose radius
19	23	Run 7-3; $\frac{H_w}{H_e}$ = 0.60; sphere-cone; l = Nose radius

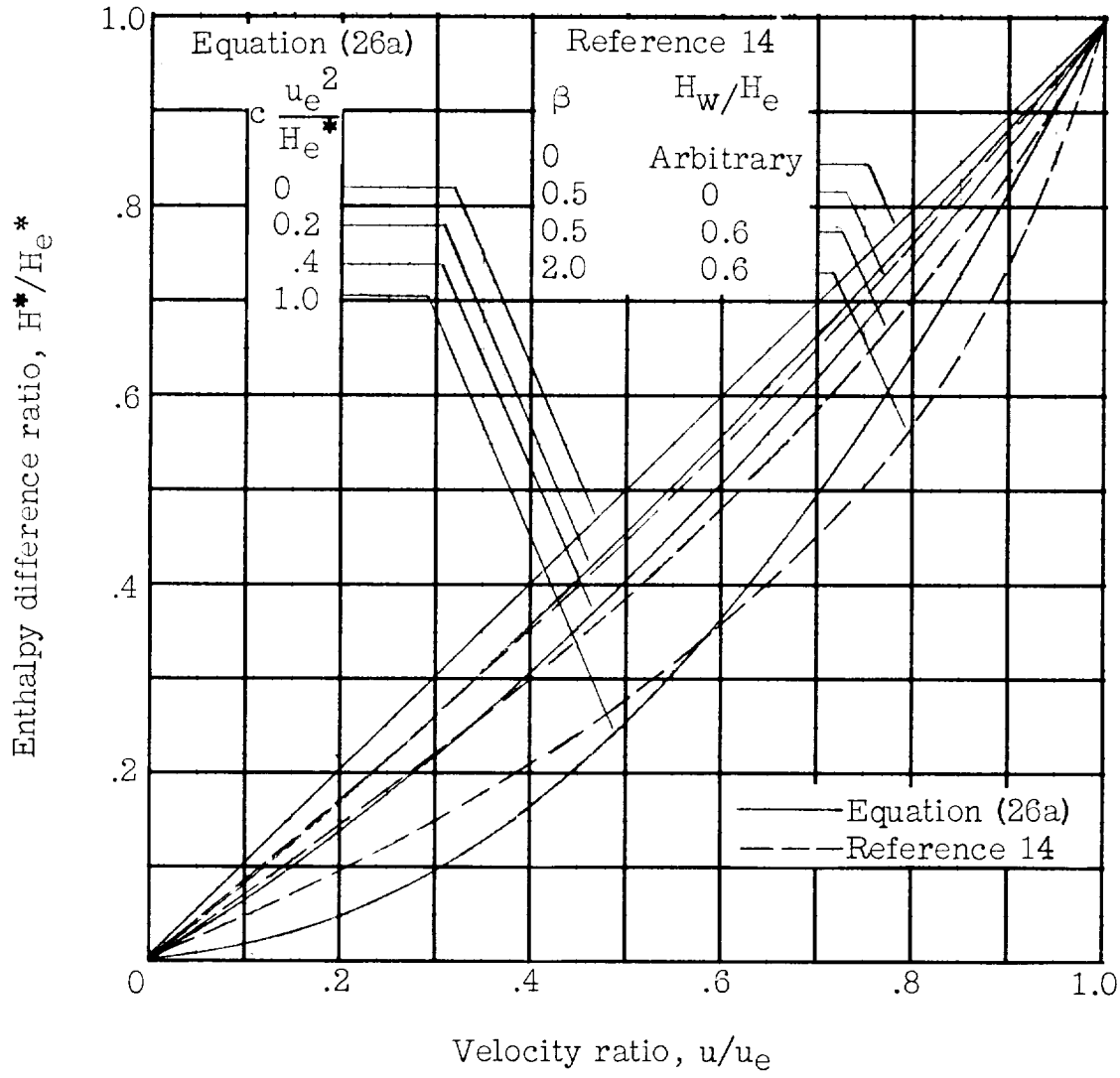

Figure 1.- Variation of enthalpy difference ratio with velocity ratio in boundary layer for present method and that of reference 14.

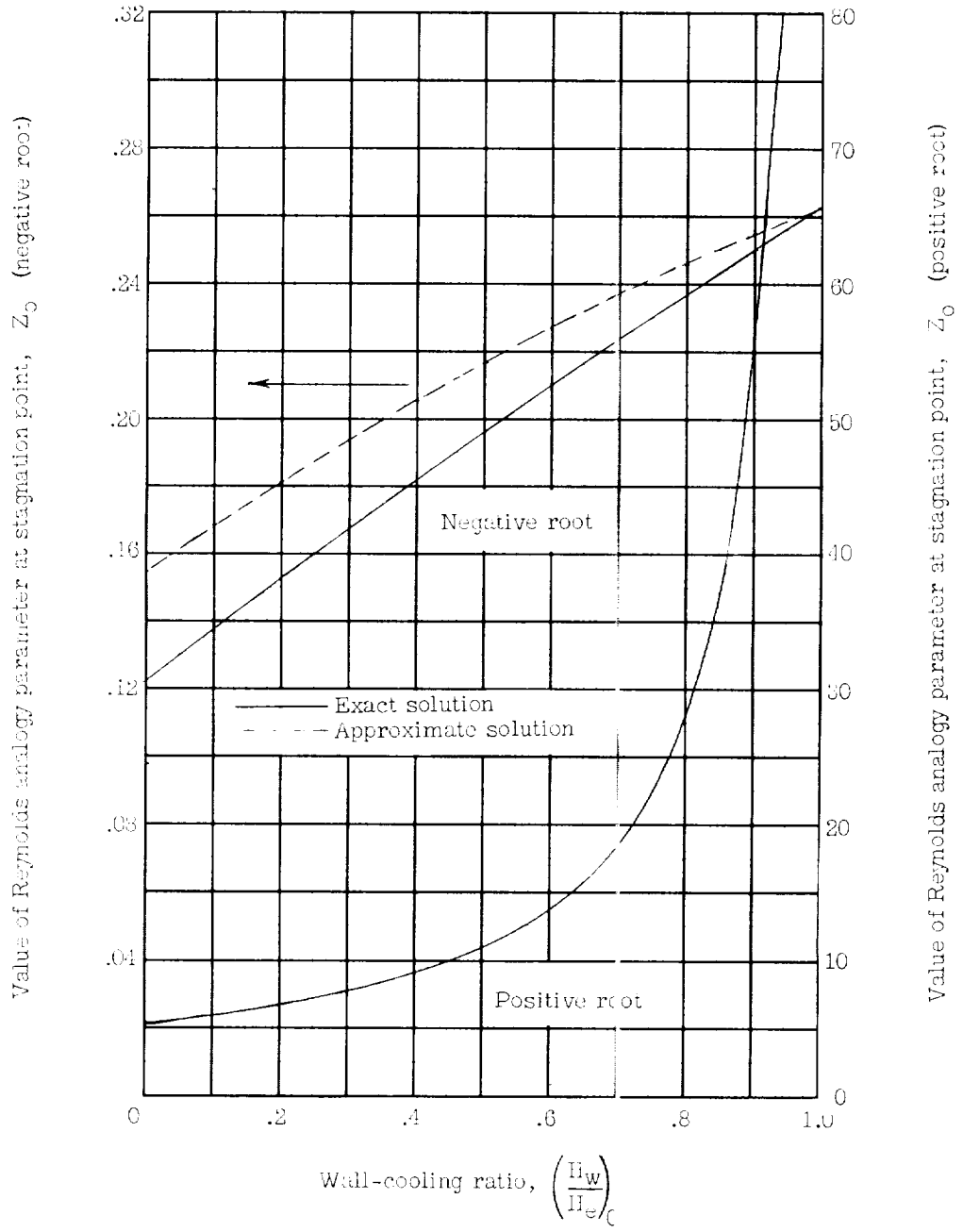

(a) Three-dimensional.

Figure 2.- Variation of stagnation-point values of Reynolds analogy parameter Z_0 with wall cooling ratio $(H_w/H_e)_0$. α = i; m = 4; n = 7.

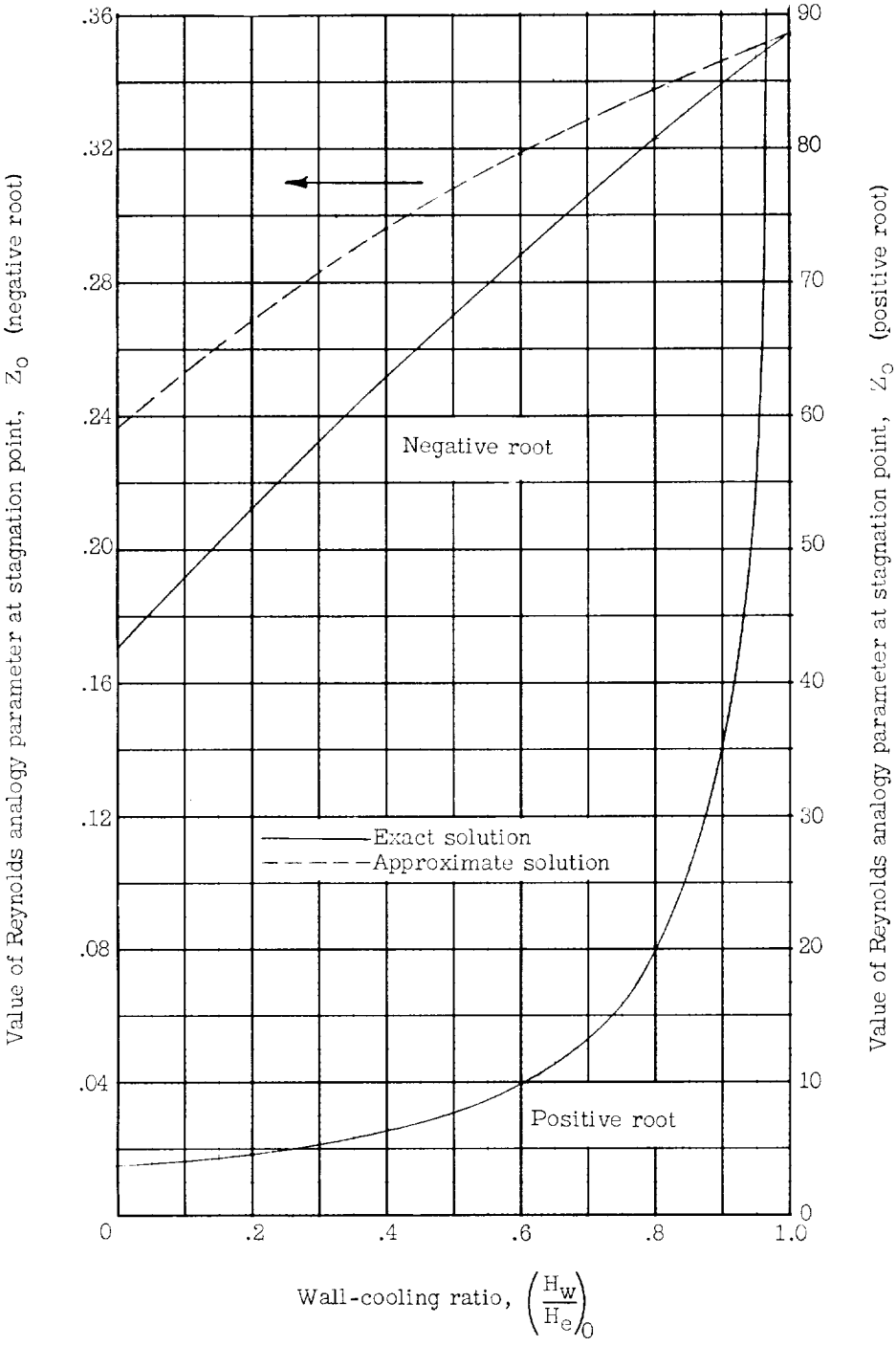

(b) Two-dimensional.

Figure 2.- Concluded.

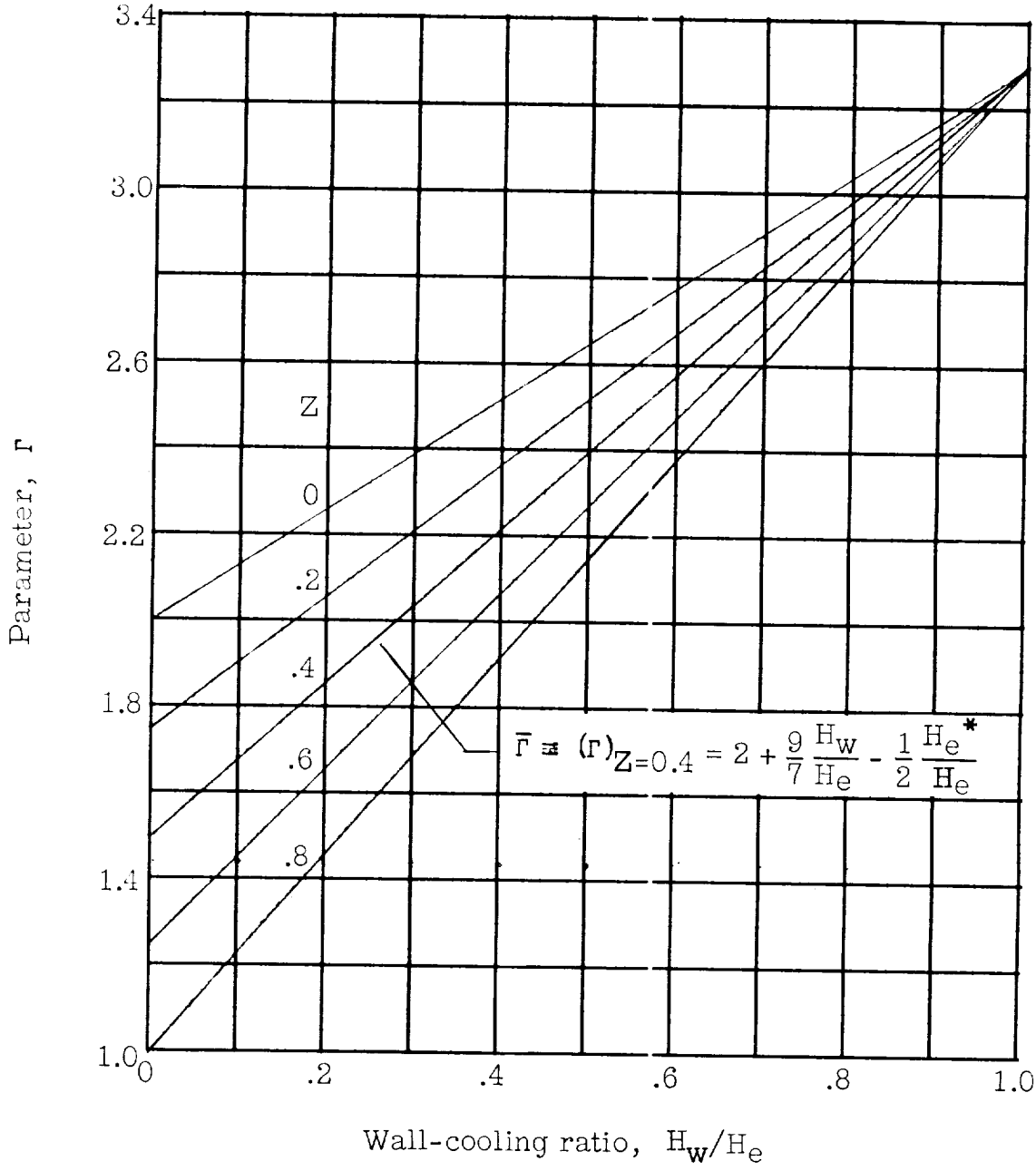

Figure 3.- Variation of parameter Γ with wall cooling ratio H_w/H_e for various values of Z. $\alpha = 1$; $n = 7$.

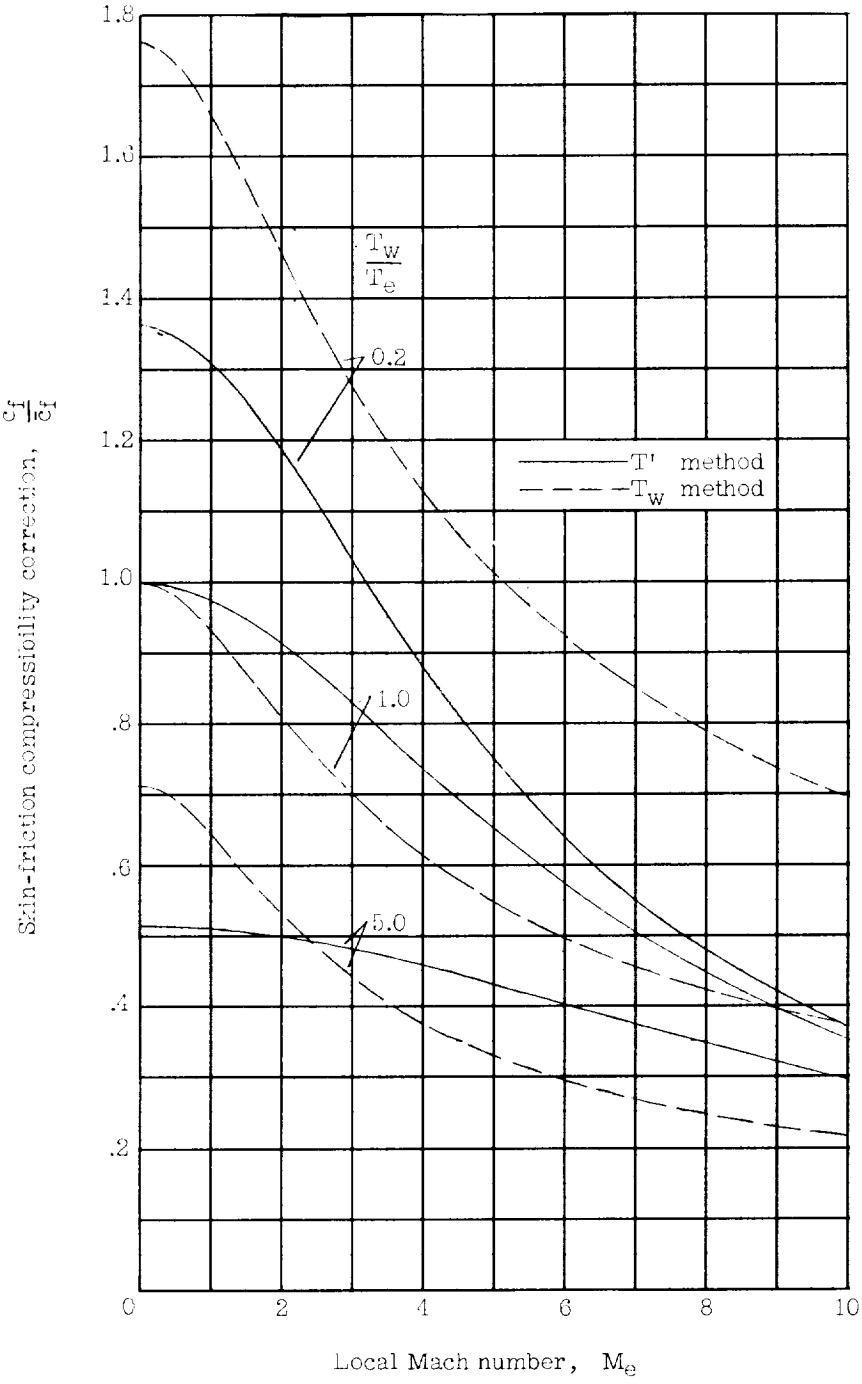

Figure 4.- Variation of flat-plate skin-friction compressibility correction with local Mach number for various wall- to stream-temperature ratios. T_w = 1,500° R.

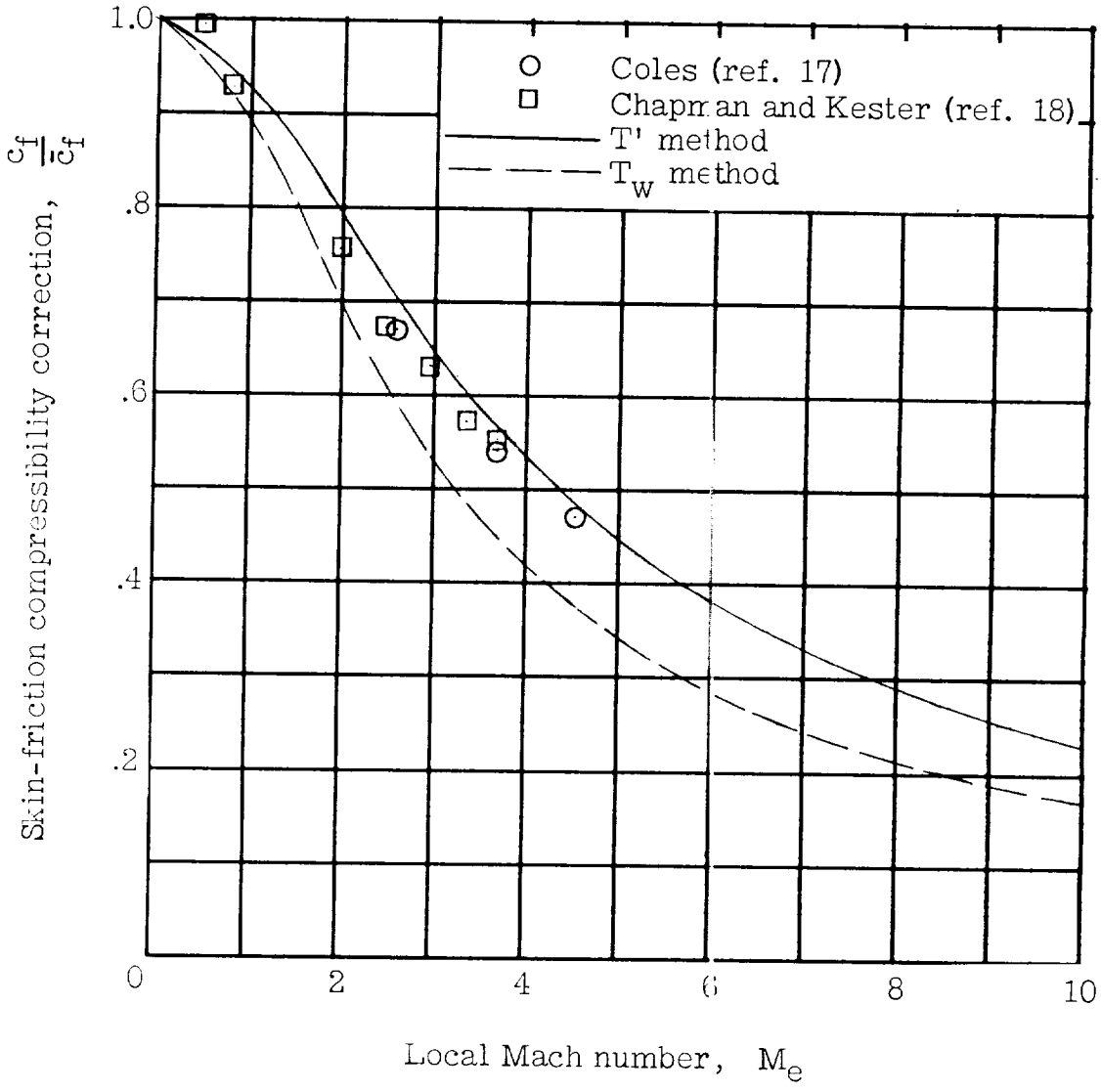

Figure 5.- Variation of skin-friction compressibility correction with local Mach number for an insulated flat plate. $T_o = 540^o$ R.

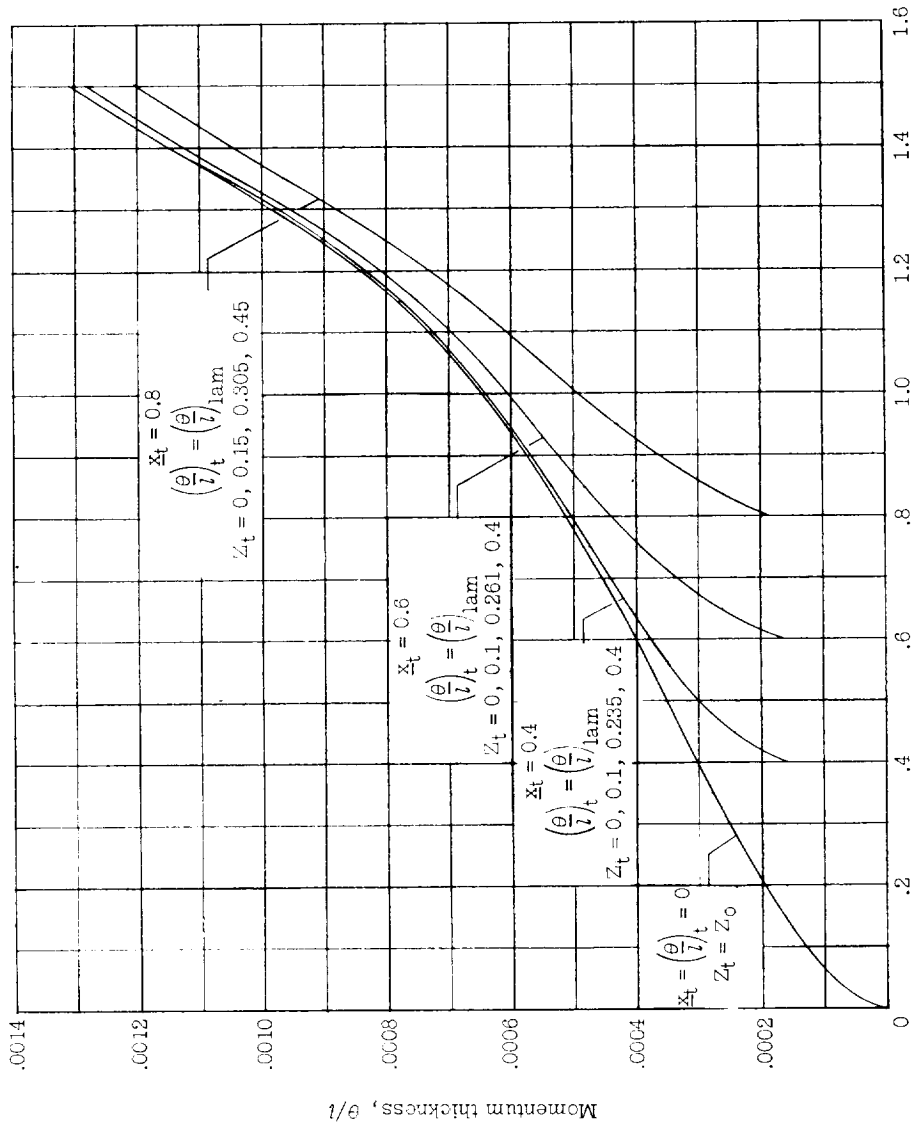

Figure 6.- Distribution of momentum thickness for hemisphere for various values of Z_t.

$$\left(\frac{\theta}{l}\right)_t = \left(\frac{\theta}{l}\right)_{laminar}; \ \bar{x}_t = 0.4, \ 0.6, \text{ and } 0.8.$$

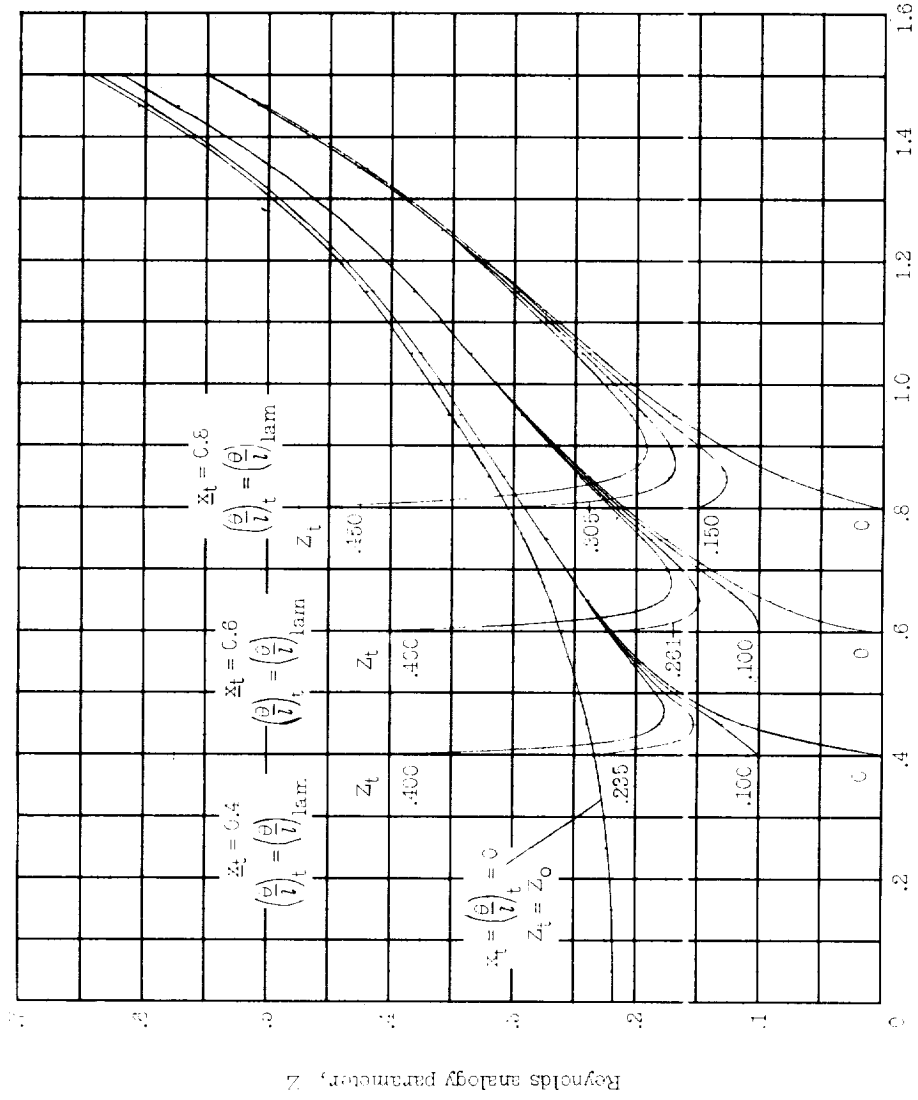

Figure 7.- Distribution of Reynolds analogy parameter for hemisphere for various values of Z_t.

$$\left(\frac{\theta}{l}\right)_t = \left(\frac{\theta}{l}\right)_{laminar}; \bar{x}_t = 0.4, 0.6, \text{ and } 0.8.$$

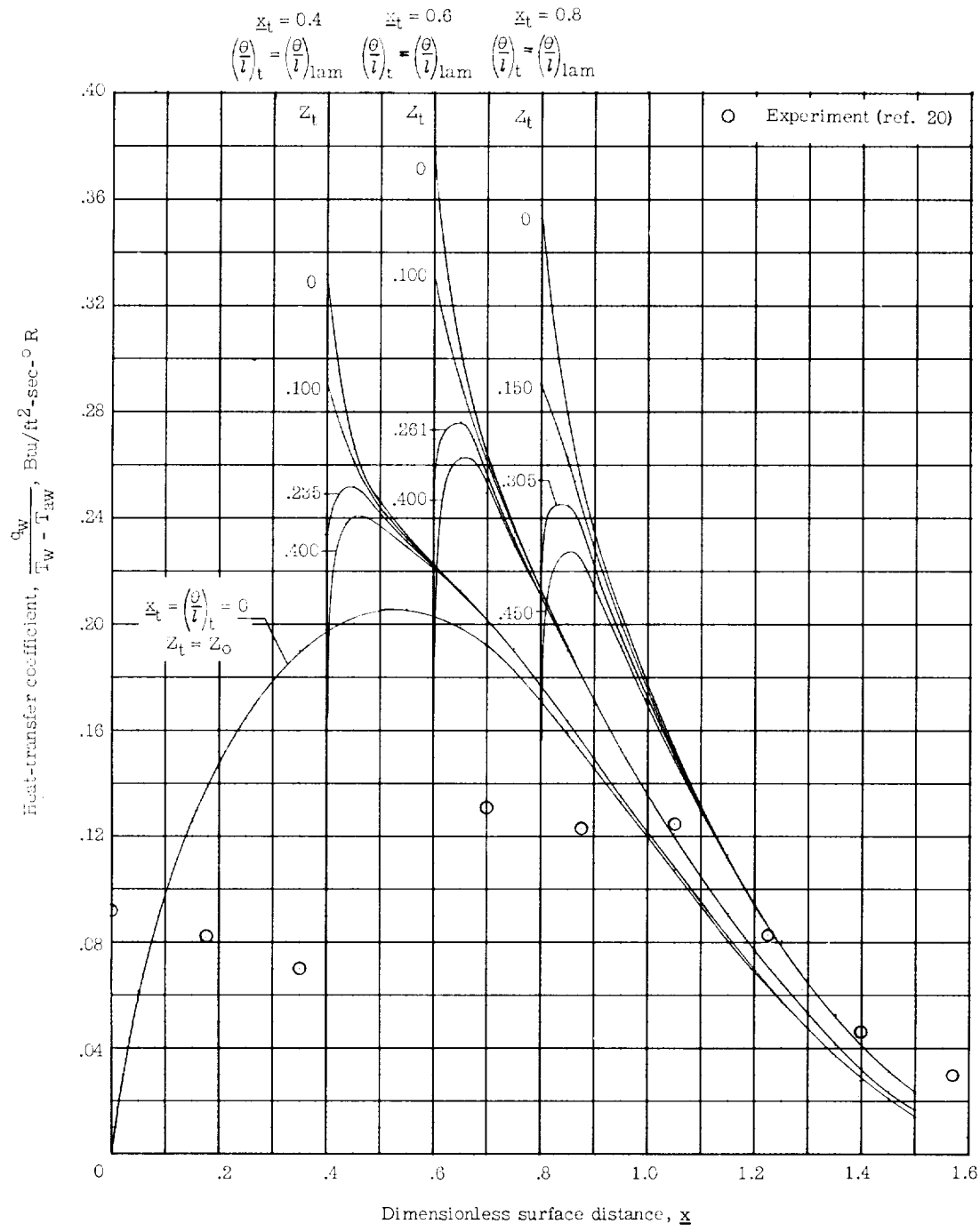

Figure 8.- Distribution of heat-transfer coefficient for hemisphere for various values of Z_t. $\left(\frac{\theta}{l}\right)_t = \left(\frac{\theta}{l}\right)_{laminar}$; $\underline{x}_t$ = 0.4, 0.6, and 0.8.

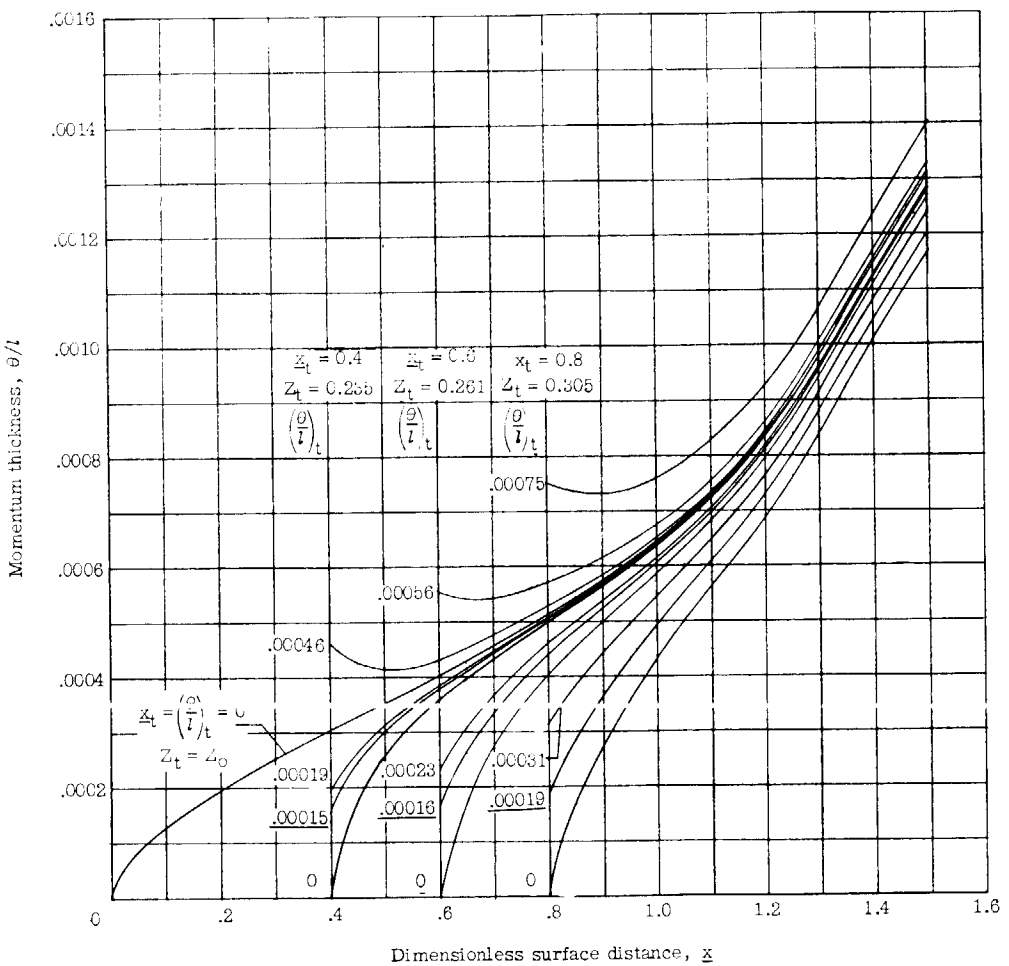

Figure 9.- Distribution of momentum thickness for hemisphere for various values of $\left(\frac{\theta}{l}\right)_t$. $\underline{x}_t$ = 0.4, 0.6, and 0.8. Underlined values of $\left(\frac{\theta}{l}\right)_t$ represent $\left(\frac{\theta}{l}\right)_{laminar}$.

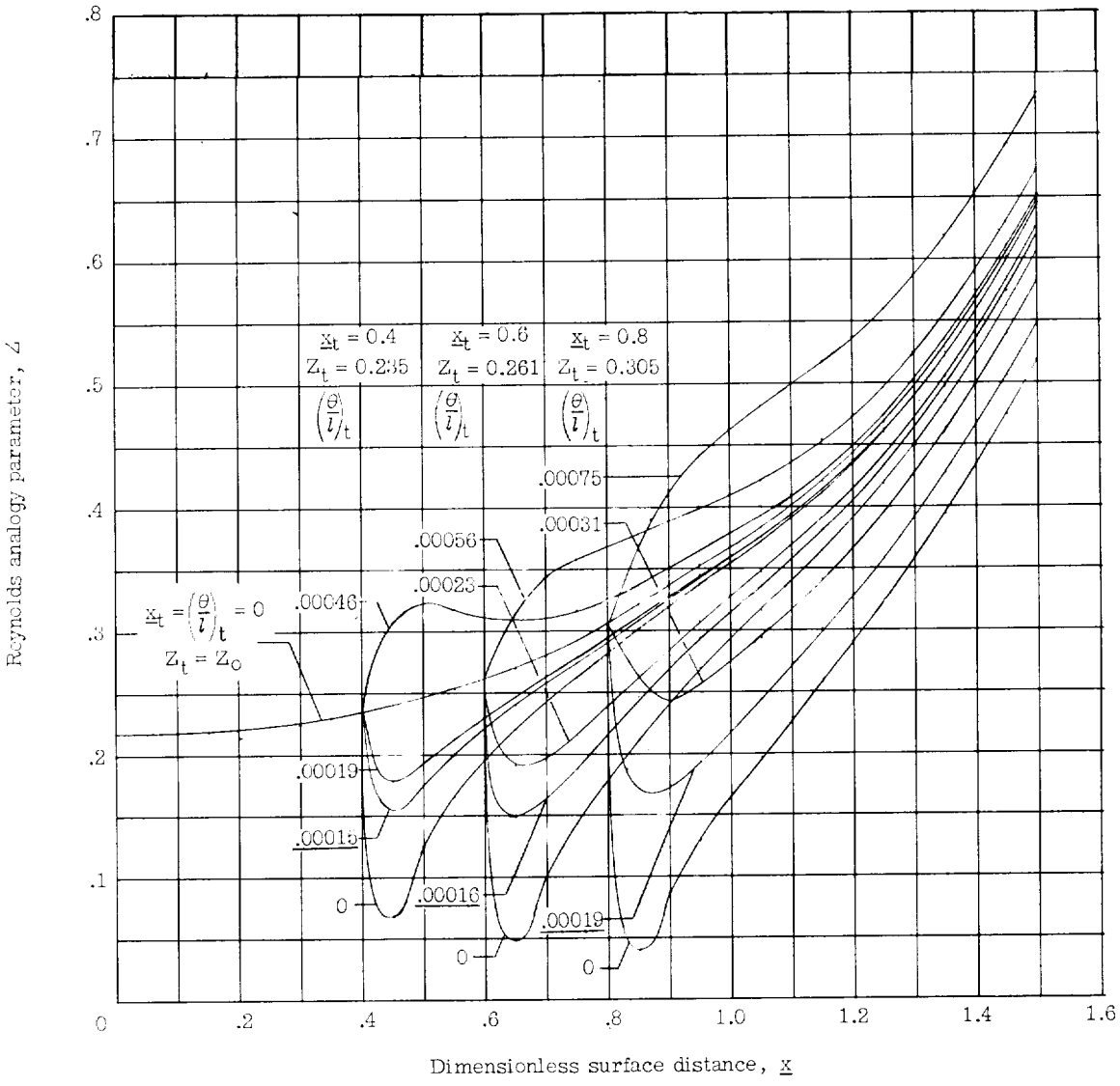

Figure 10.- Distribution of Reynolds analogy parameter for hemisphere for various values of $\left(\frac{\theta}{l}\right)_t$. $\underline{x}_t$ = 0.4, 0.6, and 0.8. Underlined values of $\left(\frac{\theta}{l}\right)_t$ represent $\left(\frac{\theta}{l}\right)_{laminar}$.

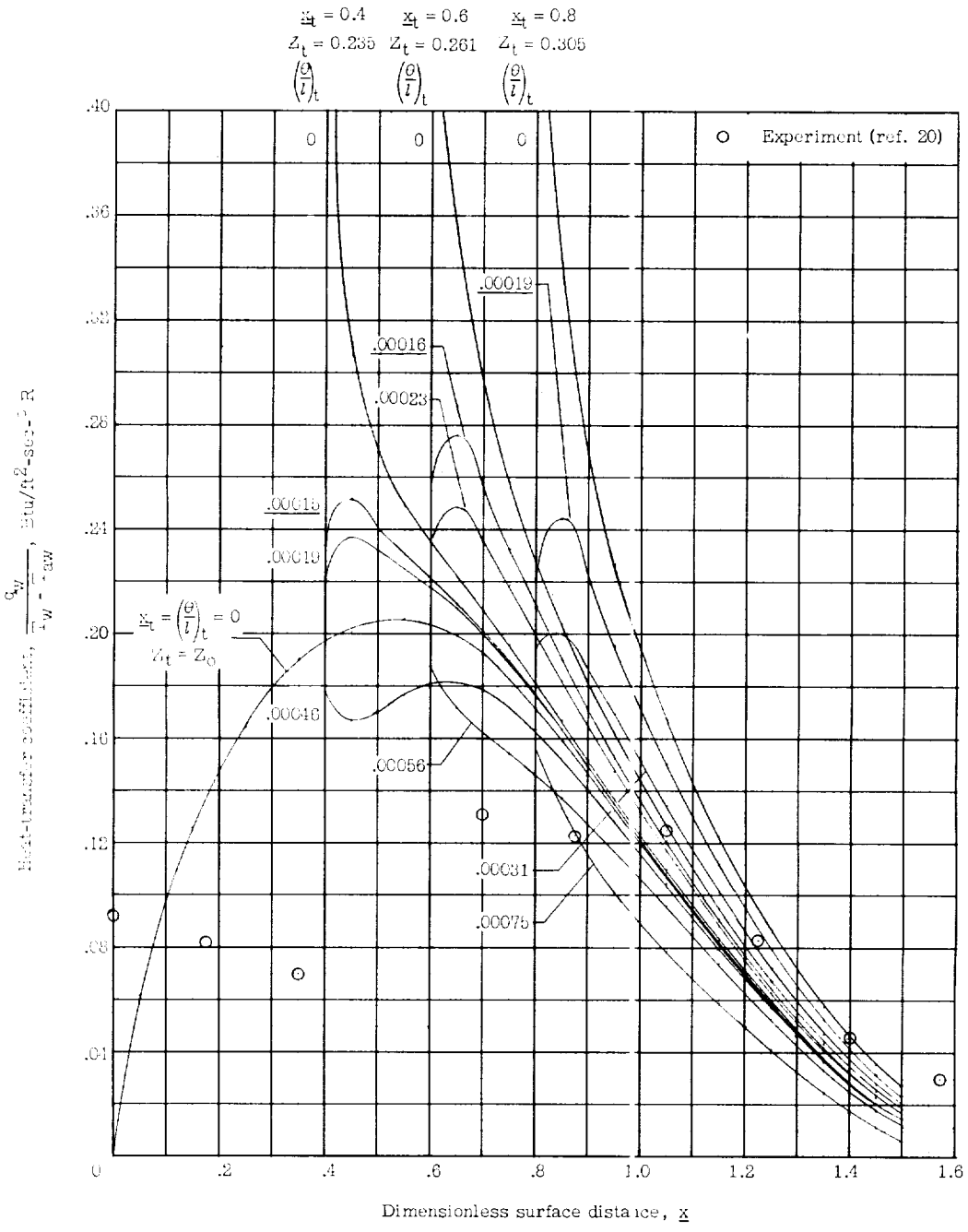

Figure 11.- Distribution of heat-transfer coefficient for hemisphere for various values of $\left(\frac{\theta}{l}\right)_t$. $\underline{x}_t$ = 0.4, 0.6, and 0.8. Underlined values of $\left(\frac{\theta}{l}\right)_t$ represent $\left(\frac{\theta}{l}\right)_{laminar}$.

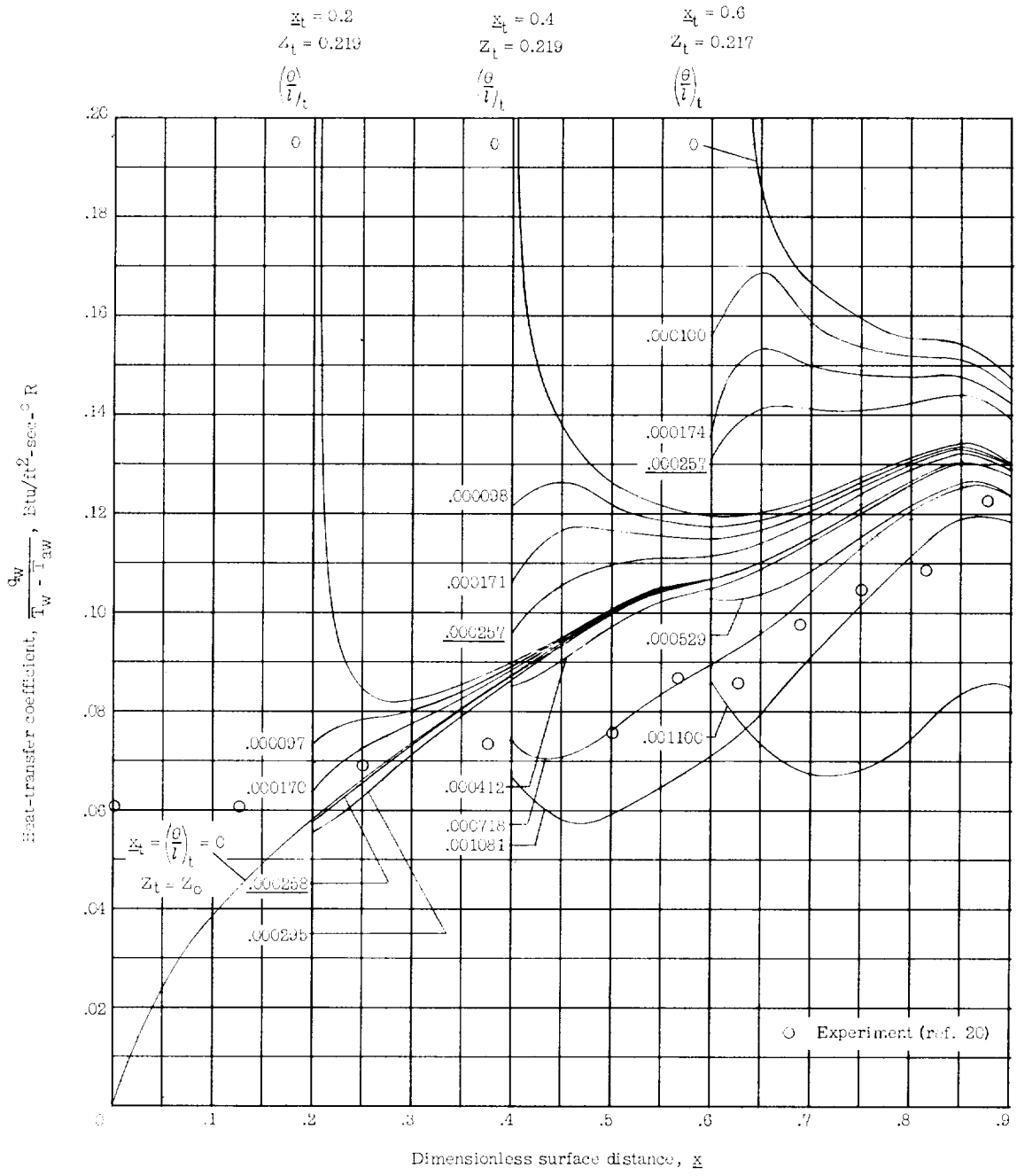

Figure 12.- Distribution of heat-transfer coefficient for flat-faced body for various values of $\left(\frac{\theta}{l}\right)_t$. $\underline{x}_t$ = 0.2, 0.4, and 0.6. Underlined values of $\left(\frac{\theta}{l}\right)_t$ represent $\left(\frac{\theta}{l}\right)_{laminar}$.

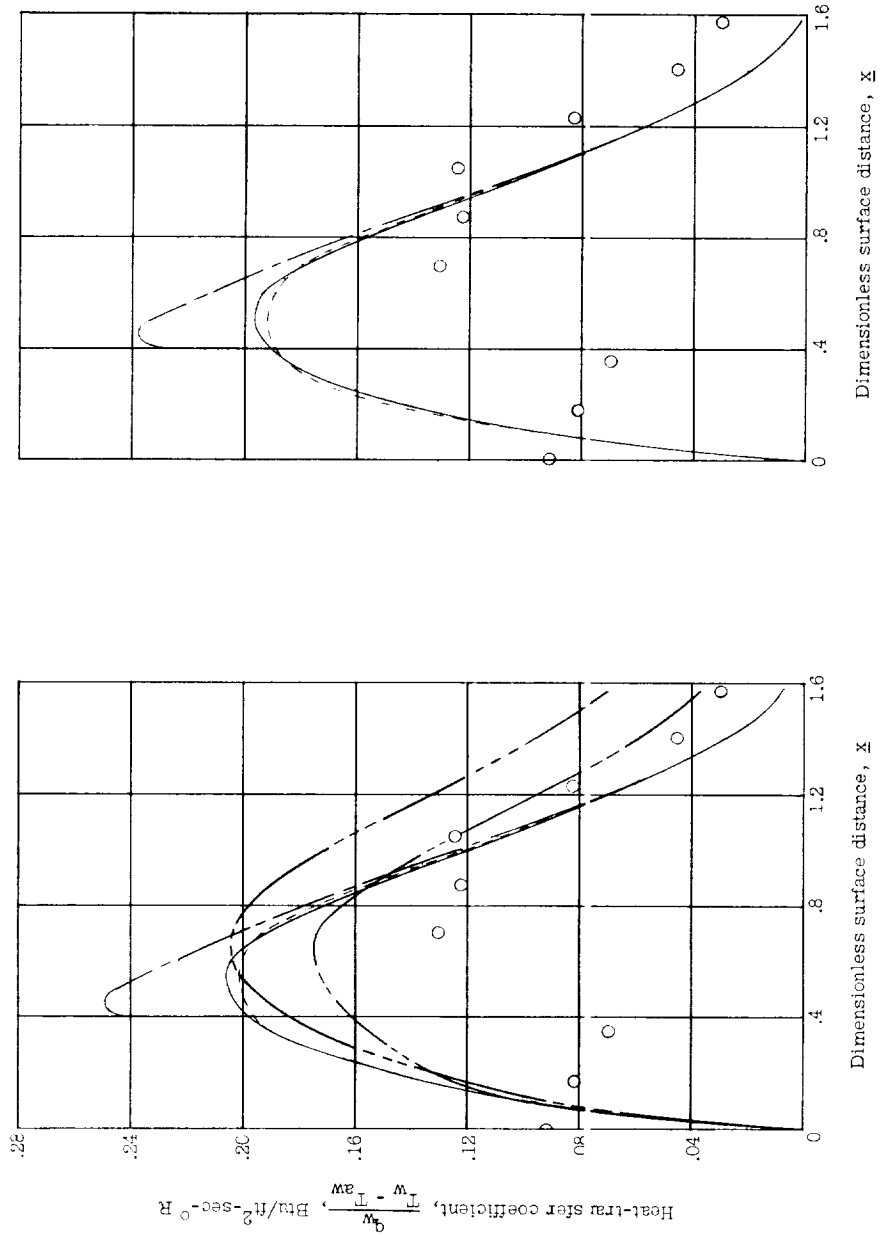

(a) T' method. (b) T_w method.

Figure 13.- Comparison of theory and experiment for a hemisphere in a Mach number 5 stream.

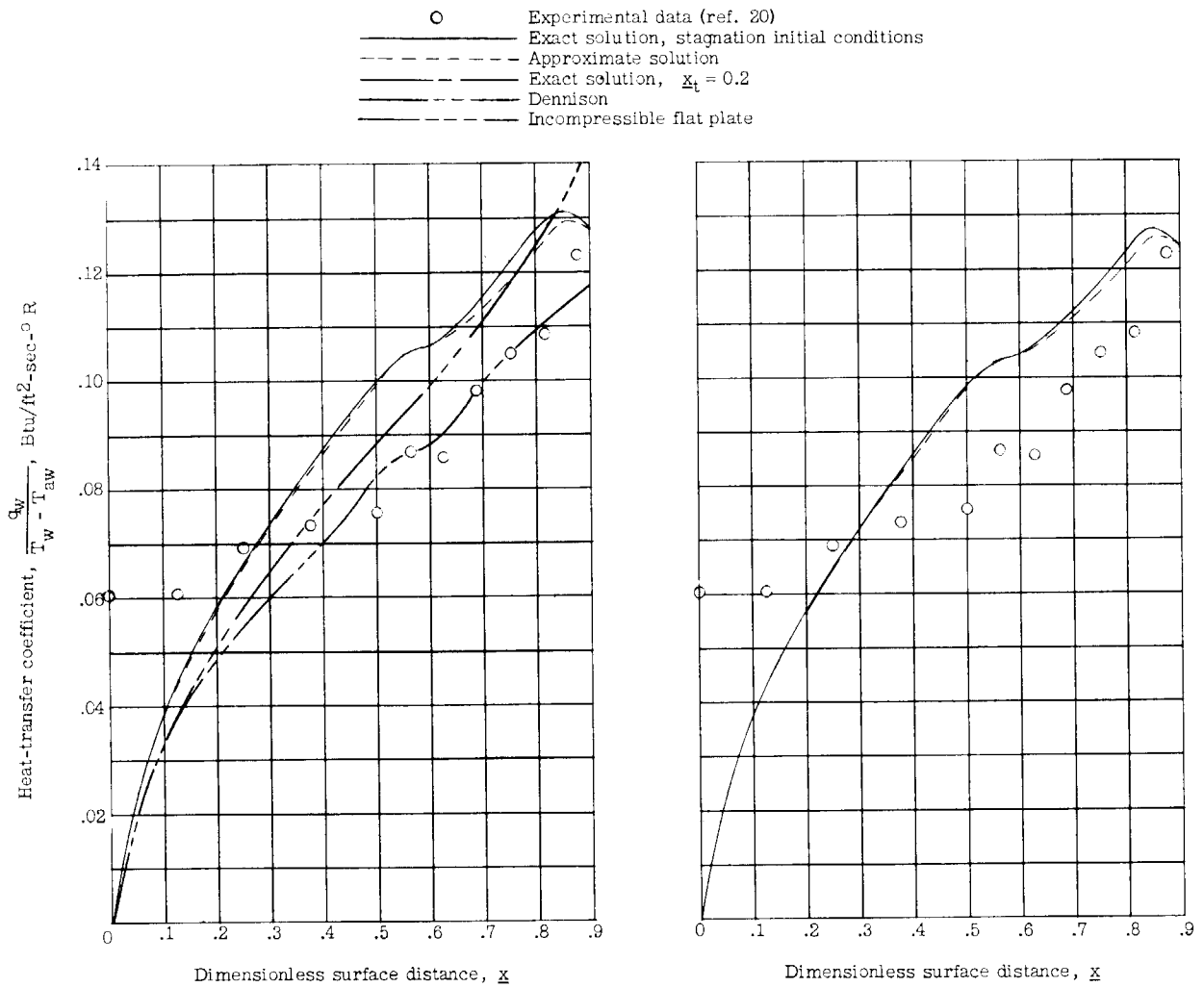

(a) T' method.

(b) T_w method.

Figure 14.- Comparison of theory and experiment for a flat-faced body in a Mach number 5 stream.

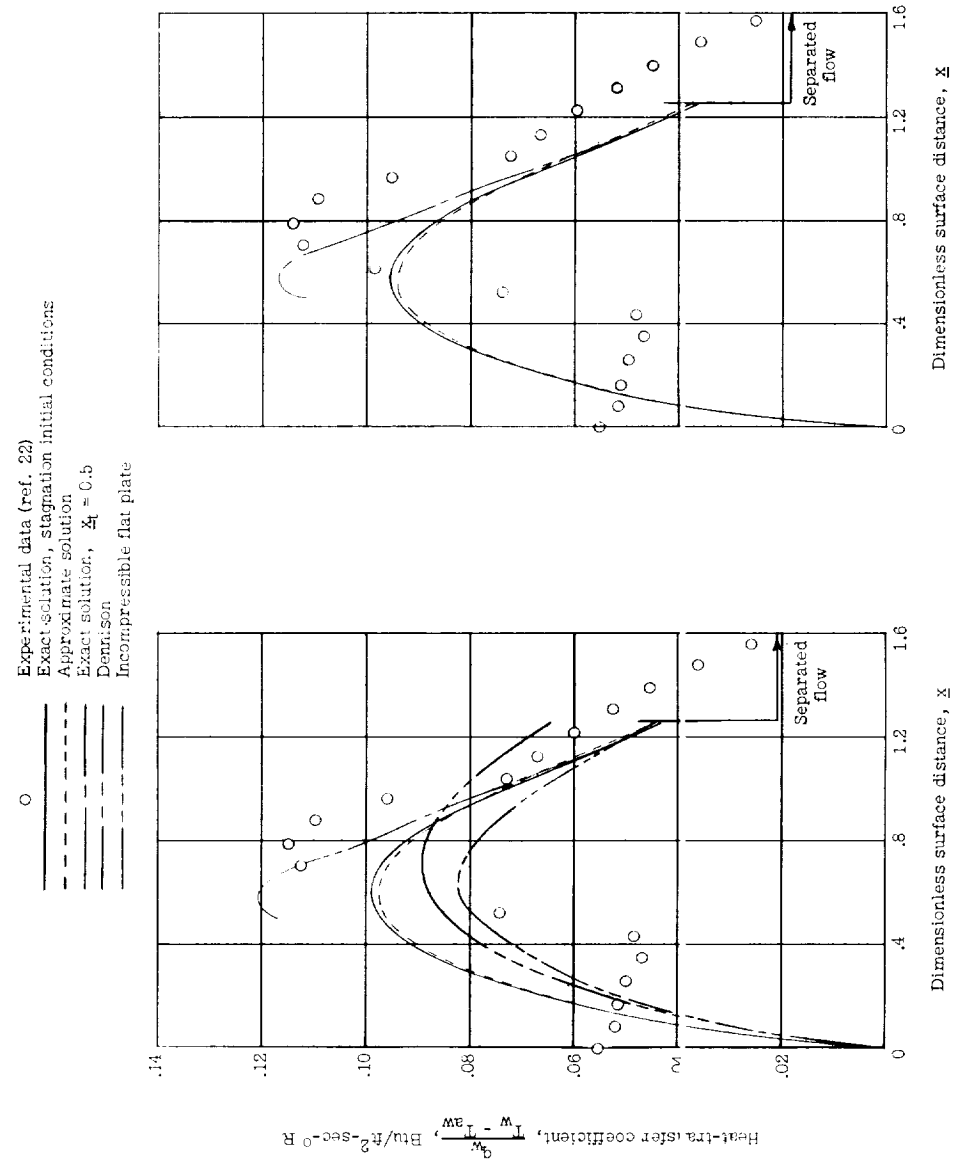

(a) T' method. (b) T_w method.

Figure 15.- Comparison of theory and experiment for a hemisphere in a Mach number 2 stream. $R_\infty = 2.74 \times 10^6$ (notation of ref. 22).

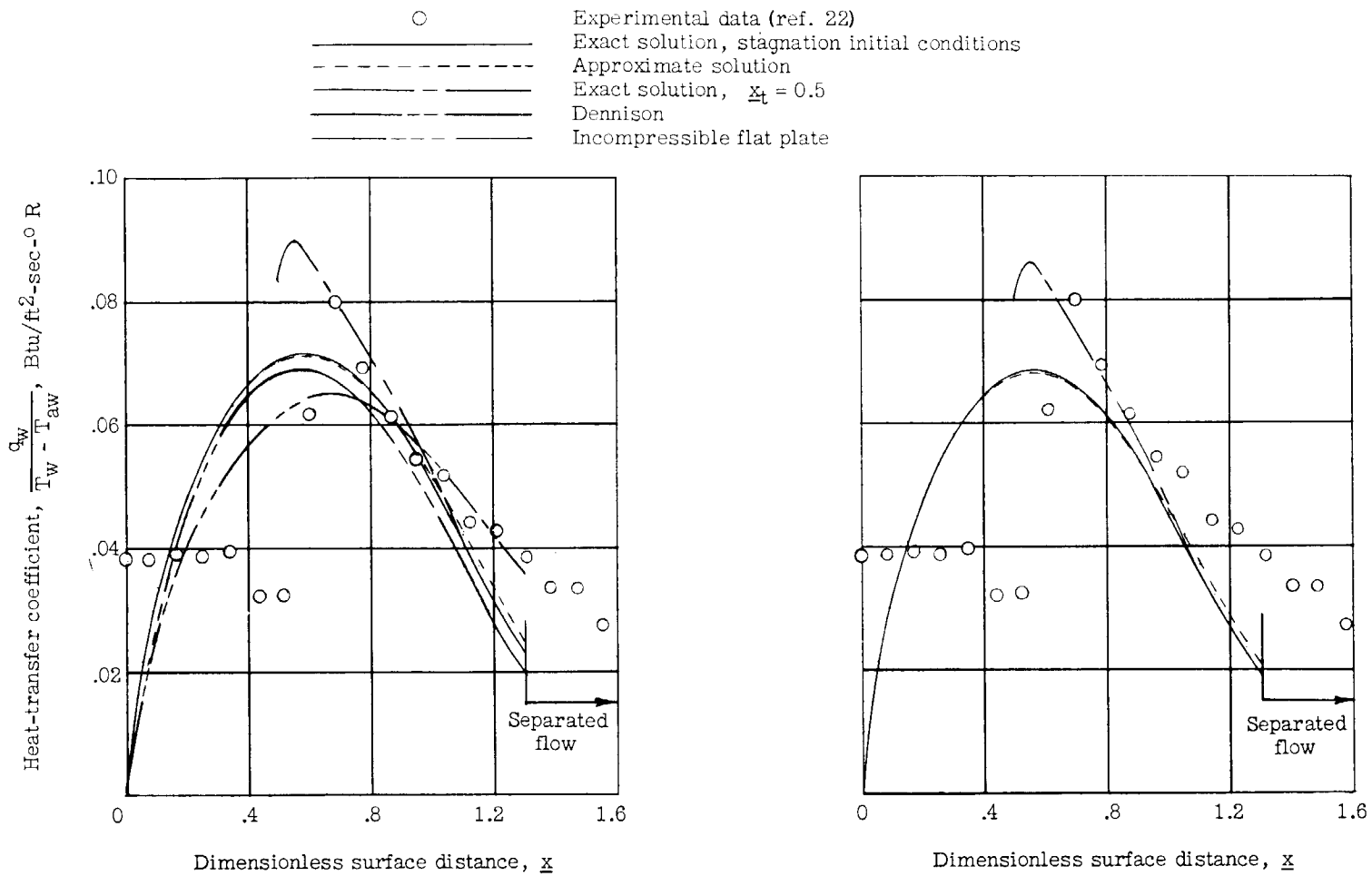

Figure 16.- Comparison of theory and experiment for a hemisphere in a Mach number 2 stream. $R_\infty = 3.50 \times 10^6$ (notation of ref. 22).

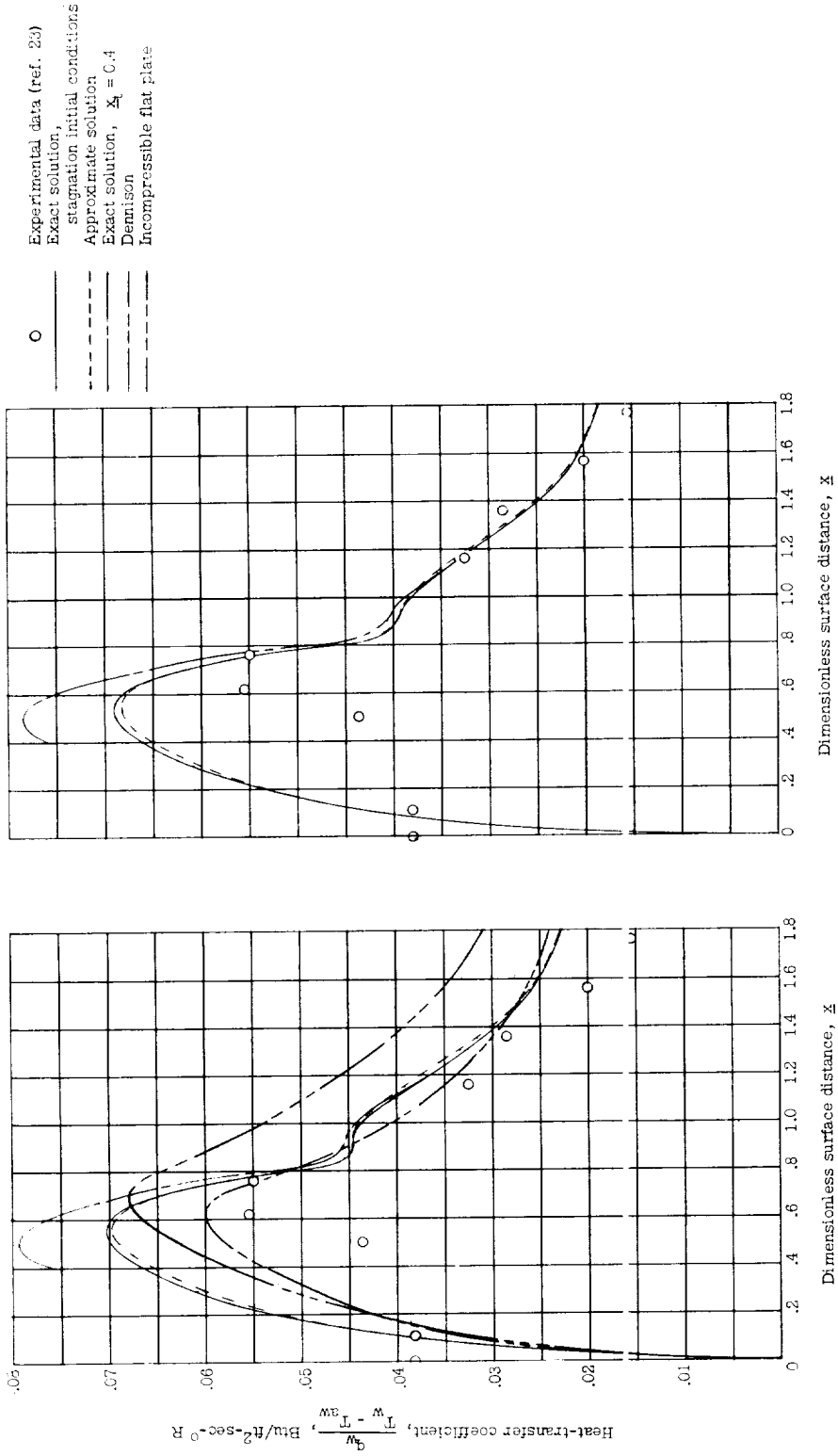

(a) T' method.

(b) T_w method.

Figure 17.- Comparison of theory and experiment for a sphere-cone in a shrouded tunnel. (Run 3-12 in ref. 23.)

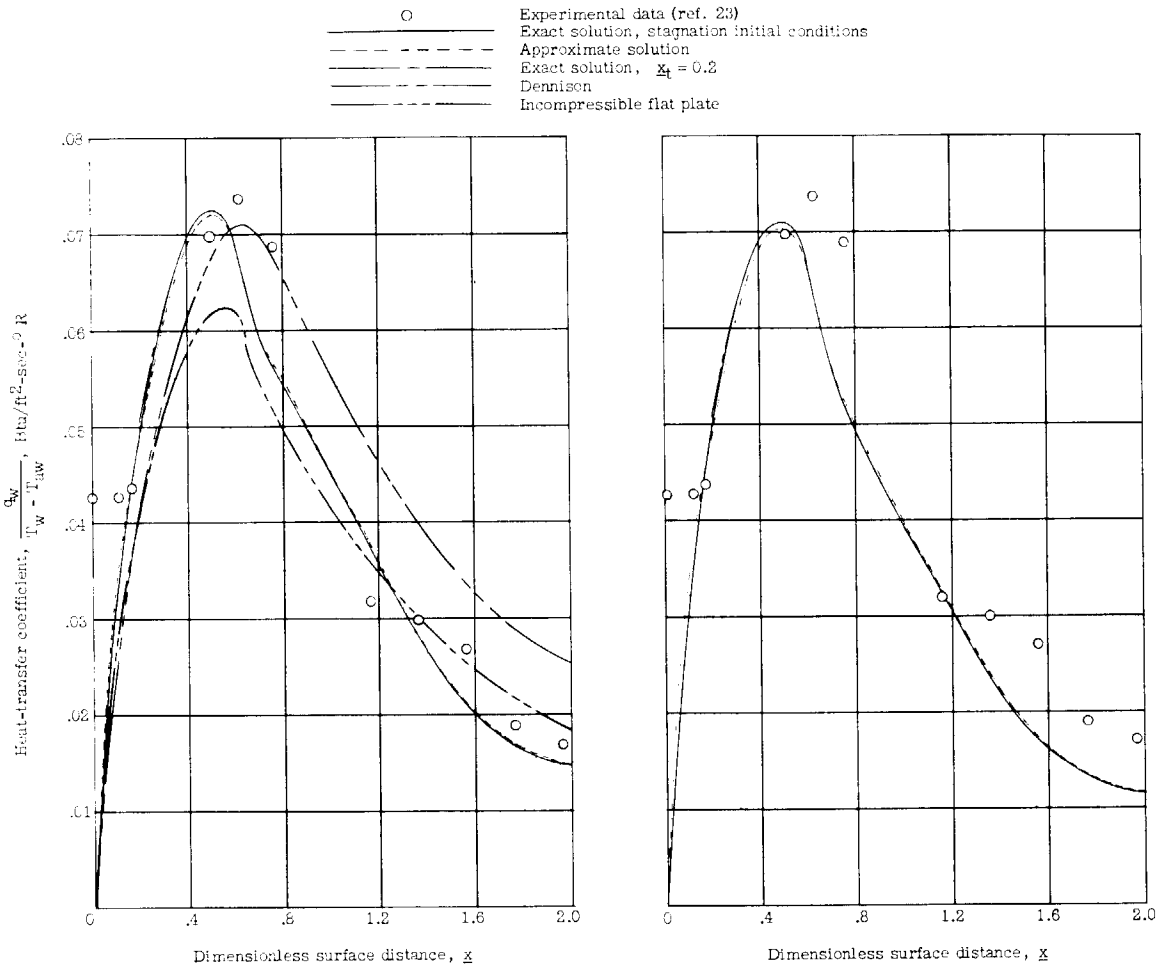

(a) T' method.

(b) T_w method.

Figure 18.- Comparison of theory and experiment for a sphere-cone in a shrouded tunnel. (Run 5-8 of ref. 23.)

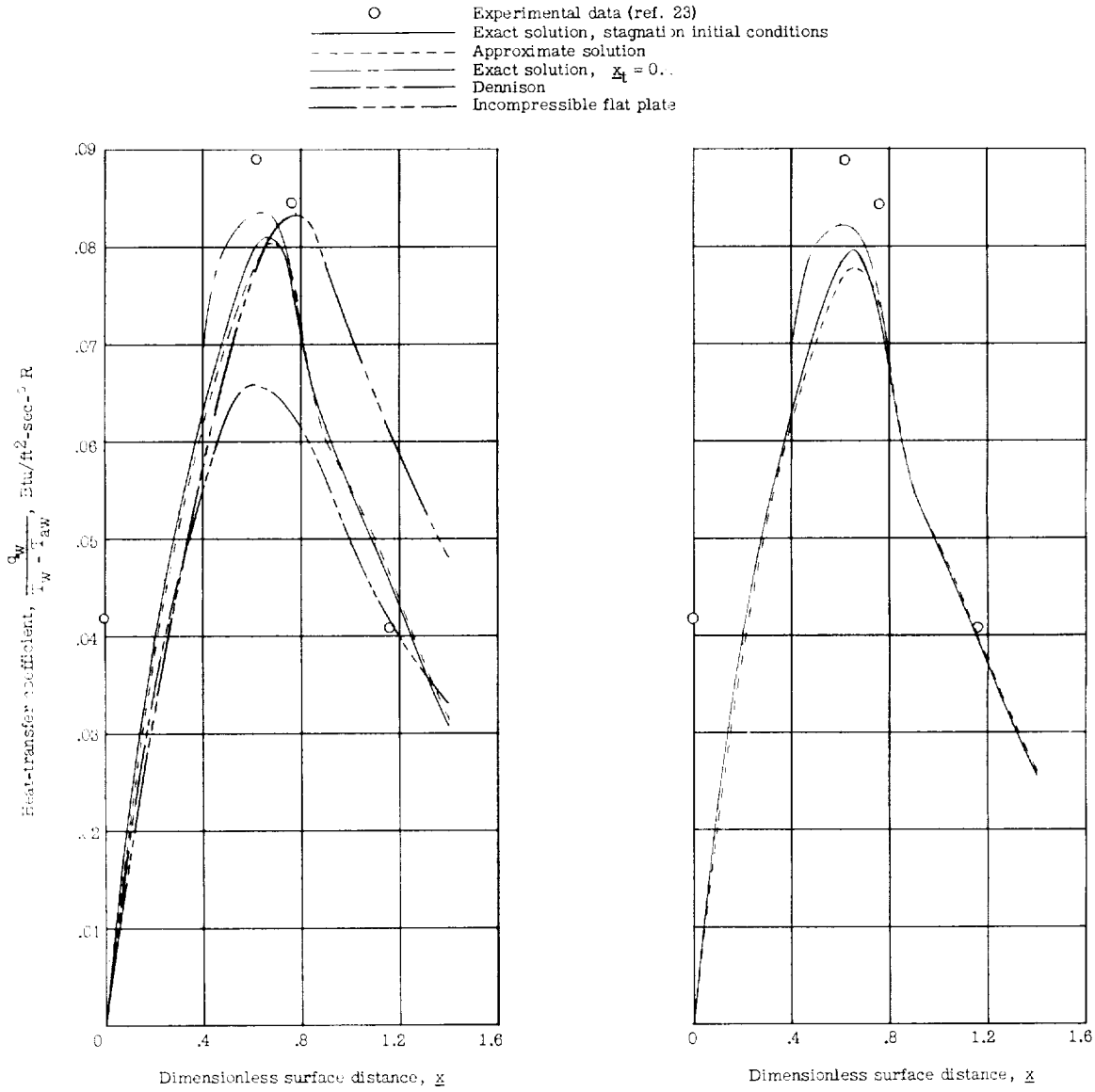

(a) T' method.

(b) T_w method.

Figure 19.- Comparison of theory and experiment for a sphere-cone in a shrouded tunnel. (Run 7-3 of ref. 23.)

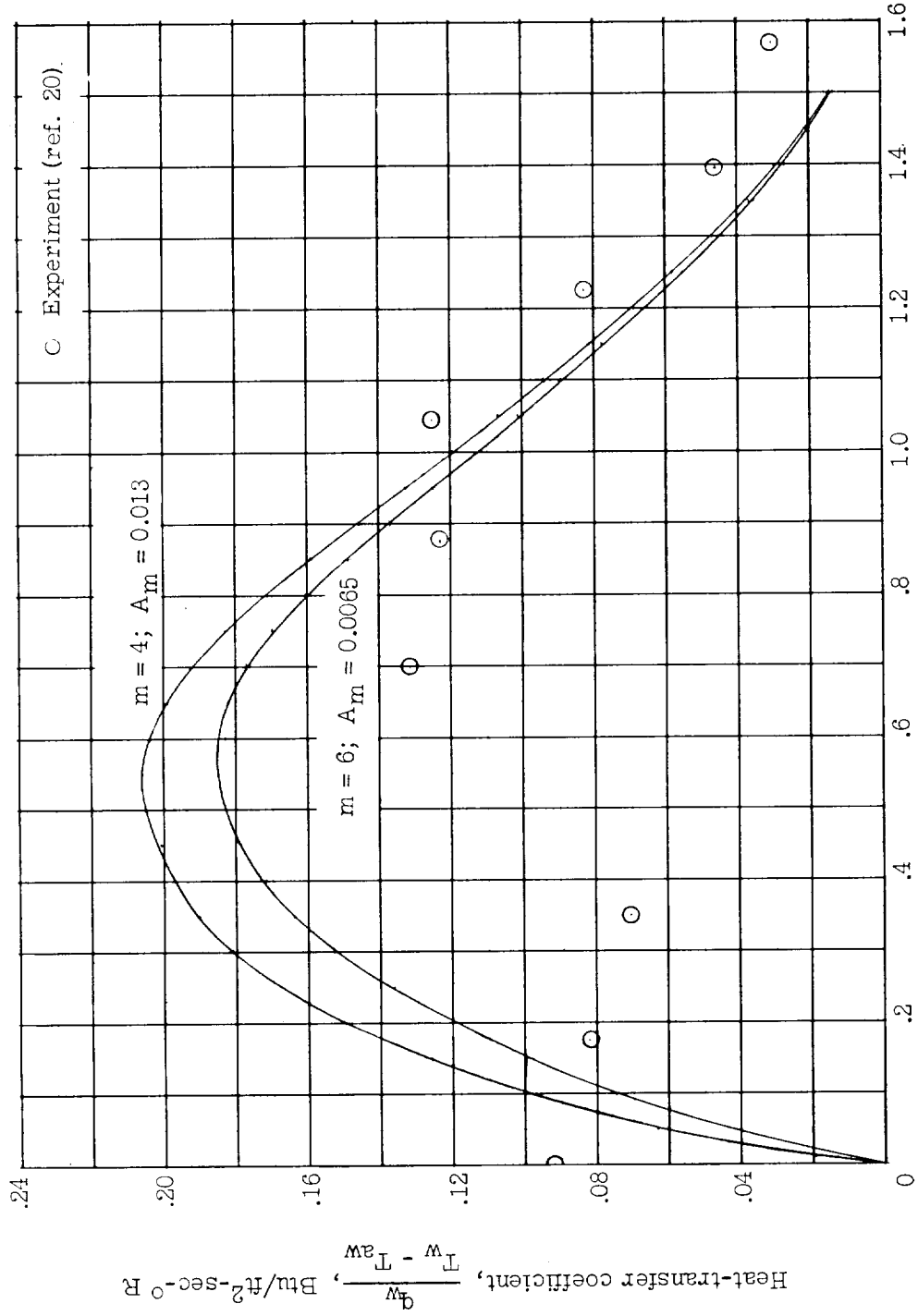

Figure 20.- Comparison of results of using two friction laws with experimental data. Hemisphere in a Mach number 5 stream; T' method.

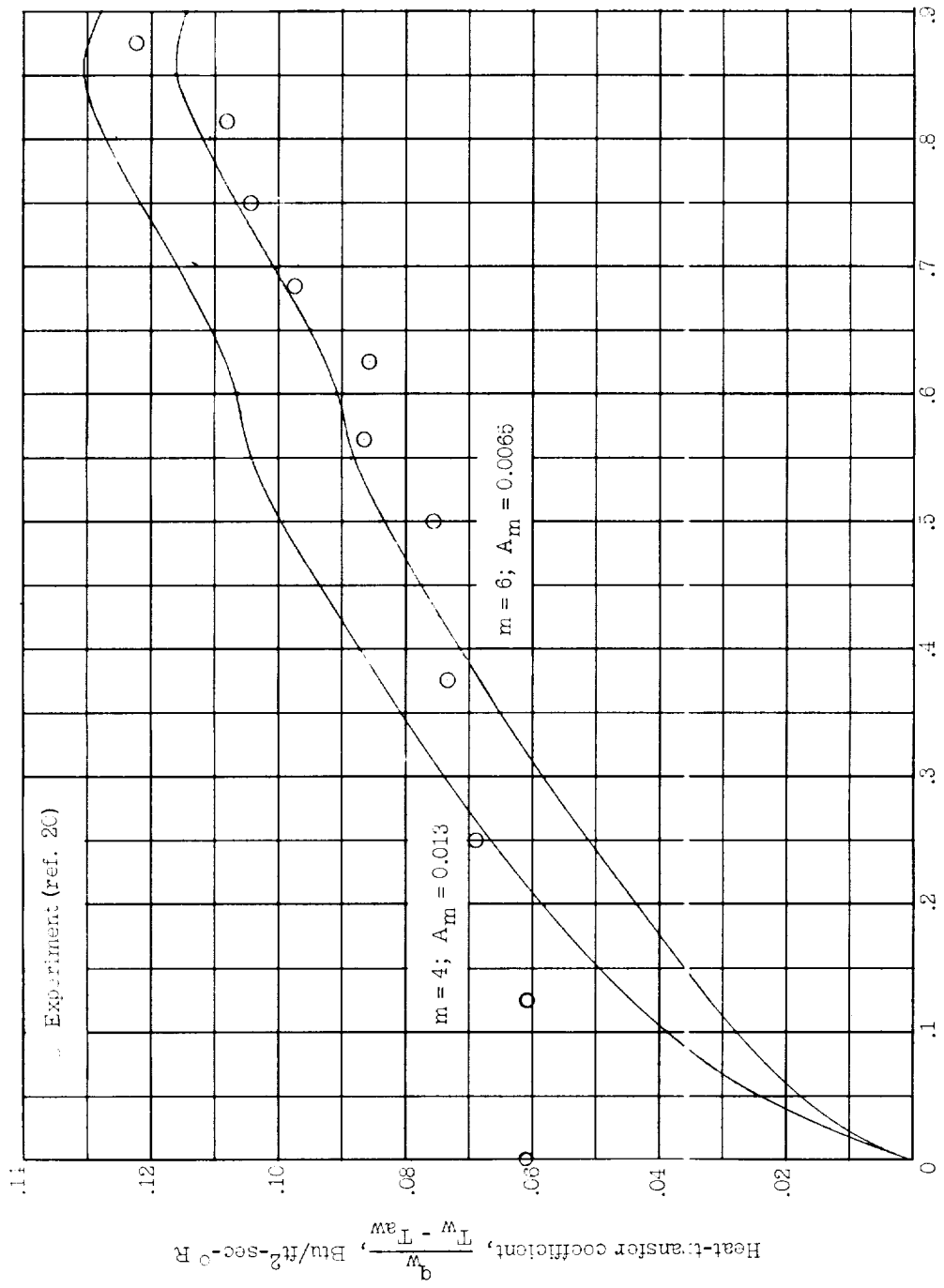

Figure 21.- Comparison of results of using two friction laws with experimental data. Flat-faced body in a Mach number 5 stream; T' method.

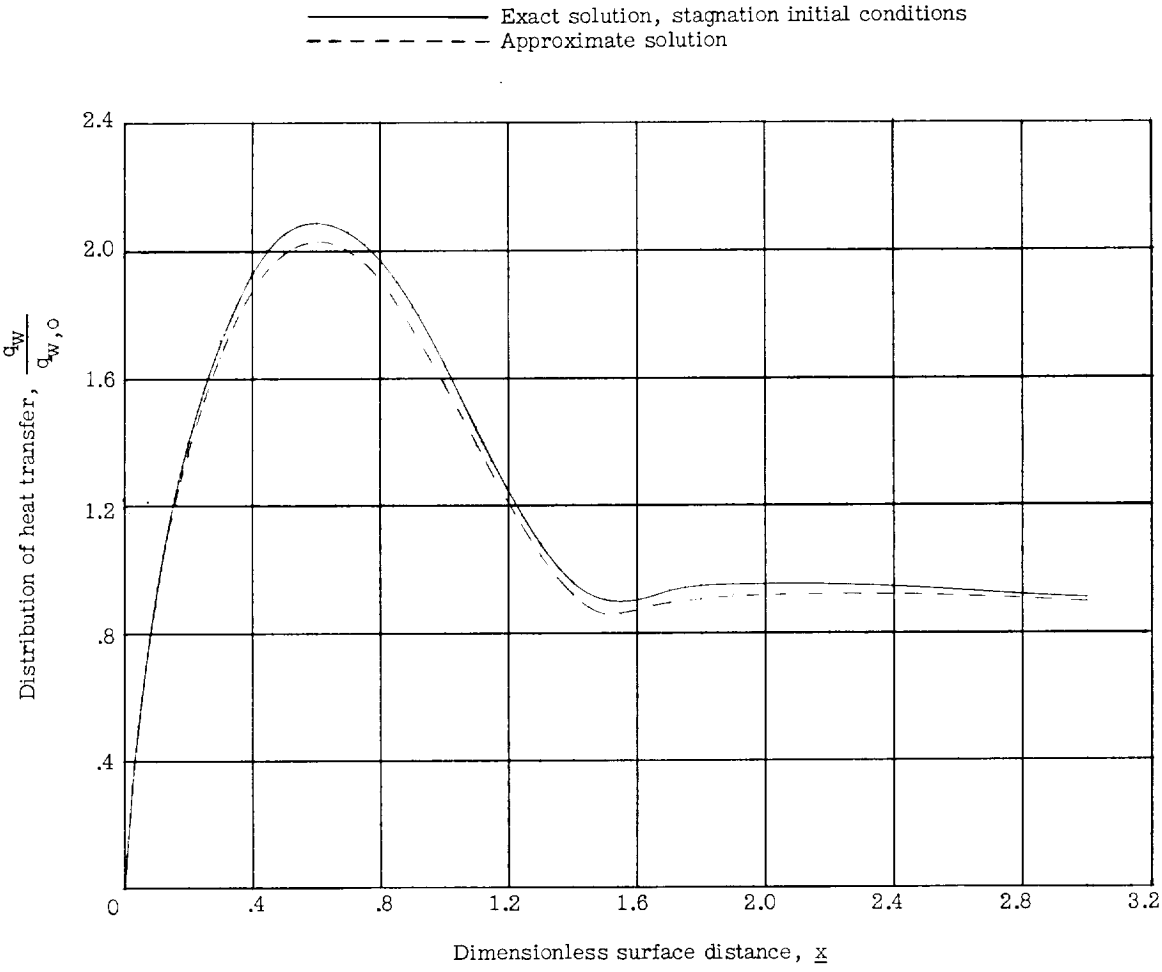

Figure 22.- Distribution of heat transfer on hemisphere cylinder for typical shock-tube flow conditions. Shock Mach number equals 6.5; pressure ahead of moving shock equals 40 centimeters mercury; T' method.